Title
C-14 Release and Transport from a Nuclear Waste Repository in an Unsaturated Medium

Authors
Light, W.B.
Zwahlen, E.D.
Pigford, T.H.
et al.

Publication Date
1990-06-01

LBL-28923
UC-814

Lawrence Berkeley Laboratory
UNIVERSITY OF CALIFORNIA

EARTH SCIENCES DIVISION

C-14 Release and Transport from a Nuclear Waste Repository in an Unsaturated Medium

W.B. Light, E.D. Zwahlen, T.H. Pigford, P.L. Chambré,
and W.W.-L. Lee

June 1990

Prepared for the U.S. Department of Energy under Contract Number DE-AC03-76SF00098

DISCLAIMER

LBL-28923

C-14 Release and Transport from a Nuclear Waste Repository in an Unsaturated Medium

W. B. Light, E. D. Zwahlen, T. H. Pigford, P. L. Chambré, and W. W.-L. Lee

Department of Nuclear Engineering
University of California

and

Earth Sciences Division
Lawrence Berkeley Laboratory
University of California
Berkeley, California 94720

June 1990

This work was supported in part by the Director, Office of Civilian Radioactive Waste Management, Office of Systems Integration and Regulations, Licensing and Compliance Division, of the U.S. Department of Energy under Contract No. DE-AC03-76SF00098.

The authors invite comments and would appreciate being notified of any errors in the report.

T. H. Pigford
Department of Nuclear Engineering
University of California
Berkeley, CA 94720

CONTENTS

1. Introduction 1

2. Release of C-14 from Waste Containers 2

2.1 Analysis 2

2.2 Results 4

2.3 C-14 Release Rates 6

3. Far-Field Transport of C-14 8

3.1 Analysis 8

3.2 Results 11

4. Conclusions 12

Acknowledgement 13

References 13

FIGURES

Figure 1. Typical Waste Packages 14
Figure 2. Penetration in a Container Wall 15
Figure 3. Waste Package Gas and Wall Temperature 16
Figure 4. Quantity of Gas in a Container, Hole at Emplacement 17
Figure 5. Gas Flow Rate, Hole at Emplacement 18
Figure 6. Quantity of Gas in a Container, Hole at 300 Years 19
Figure 7. Gas Flow Rate, Hole at 300 Years 20
Figure 8. Fractional Release Rate with Slug Flow and Binary Diffusion 21
Figure 9. C-14 Release Rates for Various Size Holes Occurring at Emplacement 22
Figure 10. C-14 Release Rates for Various Size Holes Occurring at 300 Years 23
Figure 11. Composite C-14 Release Rates for Holes at 0 and 300 Years 24
Figure 12. Gas Movement in a Fractured Porous Medium 25
Figure 13. C-14 in Pore Gas 350 m Above a Repository, Hole at 0 Year in a Single Container 26
Figure 14. C-14 in Pore Gas 350 m Above a Repository, Hole at 300 Years in a Single Container . . 27
Figure 15. C-14 Flux at Ground Surface, Hole at 300 Years, Effect of Saturation 28
Figure 16. Annual Release and Dose of C-14 at Ground Surface, Hole at 0 or 300 Years 29
Figure 17. Flux and Dose of C-14 at Ground Surface, Hole at 0 or 300 Years 30
Figure 18. Cumulative Releases of C-14 at Ground Surface, Hole at 0 or 300 Years 31

LBL-28923
June 1990

C-14 Release and Transport from a Nuclear Waste Repository in an Unsaturated Medium

W. B. Light, E. D. Zwahlen, T. H. Pigford, P. L. Chambré & W. W.-L. Lee

Department of Nuclear Engineering
University of California
and
Lawrence Berkeley Laboratory, University of California
Berkeley, CA 94720-0001

1. INTRODUCTION

This report is a preliminary total system performance analysis for a gaseous radioactive species such as $^{14}CO_2$. We study the release of ^{14}C released as $^{14}CO_2$ from partly failed nuclear waste containers by analyzing the flow of gas into and out of the container. We analyze the transport of released $^{14}CO_2$ in an unsaturated, fractured, porous medium with gas-phase advection and dispersion. We calculate the cumulative release of ^{14}C from the entire repository and inhalation dose to a maximally exposed individual, based on some very conservative assumptions. The resultant doses are very small when compared to background radiation doses and ^{14}C doses from natural background sources.

The potential nuclear waste repository at Yucca Mountain is to be in partially saturated rock. Released radioactive gases such as $^{14}CO_2$ could have a direct pathway to the biosphere. The entry of air into spent fuel would promote the oxidation of uranium matrix to more soluble forms. For licensing, the waste package must provide for substantially complete containment of radionuclides, including gases, for 300 to 1,000 years.

The waste containers will be filled with inert gas before they are sealed. Due to decay heat, temperature of the container increases. The increased temperature causes the gas pressure inside the container to increase, and inert gas could leak out through a penetration, carrying with it gaseous radioactive material such as $^{14}CO_2$. Because the waste cools, due to the decay of the heat source, and because of the loss of inert gas through the penetration, the pressure drops. The pressure inside the container will eventually fall below atmospheric pressure. As the waste cools further, air leaking in can volatilize additional ^{14}C and oxidize the fuel.

We presents some initial analyses of gas flow into and out of nuclear waste containers, through holes of specified timing and sizes. Also, we predict the release rate of ^{14}C.

We analyze the far-field transport of released $^{14}CO_2$ in an unsaturated, fractured, porous medium with gas-phase advection and dispersion. Gases released into a partially saturated, fractured rock tend to move in fractures, but some species are retarded by absorption in vadose water inside the rock matrix. Strong convection flow of gas is expected during the thermal phase of repository operation, carrying $^{14}CO_2$ more rapidly toward the ground surface.

First we assess the interaction of $^{14}CO_2$ with vadose water as a possible retardation mechanism. We show how to treat the combined fracture and pore matrix as an equivalent porous medium, and we predict ^{14}C concentrations, fluxes, cumulative release and inhalation dose for a maximally exposed individual 350 m above the repository.

2. RELEASE OF C-14 FROM WASTE CONTAINERS

2.1 ANALYSIS

Some waste packages at Yucca Mountain will contain spent fuel assemblies or consolidated fuel rods; others will contain borosilicate glass in steel pour canisters. Figure 1 is a sketch of typical waste packages, from the *Site Characterization Plan* [USDOE 1988]. We study gas flow through penetrations modeled as a single equivalent hole of radius r and length ℓ, Figure 2. The flow regime can be characterized by the Knudsen number Kn, which is the ratio of the mean free path length λ to the hole diameter, Kn= $\lambda/2r$.

Table I shows the dominant flow regime for various Knudsen numbers.

Table I. Flow Laws for Gases as a Function of the Knudsen Number Kn

Kn	Type of Flow
$\gg 1$	Knudsen/Molecular Flow
≈ 1	Slip Flow (Transition)
$\ll 1$	Viscous Flow

The mean free path is characteristic of the gas and Table II shows some mean free paths of gases of interest.

From Table II, it can be seen that for a single hole of larger than one micrometer in diameter, viscous flow will dominate. We will show later that gas flow through holes of less than one micrometer in diameter will be negligible, under any flow law.

Table II. Mean Free Paths of Selected Gases

Gas	λ at 298 K	λ at 500 K
Air	6.6×10^{-8} m	1.1×10^{-7} m
Argon	6.9×10^{-8} m	1.2×10^{-7} m
CO_2	4.3×10^{-8} m	7.3×10^{-8} m
Krypton	5.3×10^{-8} m	8.9×10^{-8} m
Xenon	3.9×10^{-8} m	6.5×10^{-8} m

Source: Calculated using data from Kennard [1938].

Viscous Flow

The equation for steady viscous (Poiseuille) flow of an ideal gas in a tube at constant temperature is

$$Q = \frac{\pi r^4 (P^2 - P_0^2)}{16 \mu \ell R T} \tag{1}$$

Here Q is the molar flow rate of gas, P and P_0 are the gas pressures inside and outside the container, and μ is the absolute viscosity of the gas. Here we assume that the penetrations through the container wall of thickness ℓ can be approximated by a single equivalent hole of radius r and length ℓ, with the gas in local thermal equilibrium with the container wall at temperature T_w. Because the temperature in the repository changes slowly, over hundreds of years, the steady-state gas flow law is applicable. In a waste container containing n moles of gas in a gas volume V, the equation can be transformed into a differential equation in terms of n

$$\frac{dn(t)}{dt} = -\frac{\pi r^4 [(n R \bar{T}/V)^2 - P_0^2]}{16 \mu \ell R T_w} \tag{2}$$

with the initial quantity of gas given by the ideal gas law

$$n(0) = \frac{P(0) V}{R T(0)} \quad . \tag{3}$$

Here the average internal temperature $\bar{T}$, and the wall temperature T_w, are known functions of time, and μ is an empirical function of T_w. $\bar{T}$ is approximated as the arithmetic average of the time-dependent fuel cladding temperature and T_w. The time for the waste to heat to its maximum temperature after emplacement is neglected.

Knudsen/Molecular Flow

For extremely small holes, molecular flow applies

$$Q = \frac{8 \pi r^3 (p - p_0)}{3 \ell \sqrt{2 \pi m R T}} \tag{4}$$

where m is the gas molecular weight, and p and p_0 are the partial pressures of a gaseous species.

Diffusive Release

The viscous flow model neglects any diffusive release of gaseous species. As fill gas leaks out through penetrations, gaseous species will be released by advection and diffusion, both in the same direction. At later times, as the waste package cools, air begins to flow into the waste container, and gaseous species will be released by diffusion against air inflow.

When advection and diffusion are both in the same direction, advective transport of gaseous radionuclides out of the container is the dominant release process. When advection is inward and diffusion is outward, we have counter-diffusion, thus the diffusive transport of gaseous radionuclides is the only release mechanism.

We analyze counter-diffusion release through the equivalent tubular penetration, with quasi-steady-state flow and diffusion. The geometry is the same as Figure 2. Assuming slug flow and constant-concentration boundary conditions at the tube ends, the steady-state mass-balance equation for the radionuclide concentration

c in the flow tube

$$\bar{v}\frac{dc}{dz} = D\frac{d^2c}{dz^2}, \qquad 0 \le z \le \ell \tag{5}$$

with z the direction of flow along the tube, and the boundary conditions

$$c(0) = c_0 \tag{6}$$

$$c(\ell) = 0 \tag{7}$$

Here c_0 is a constant concentration of the radionuclide in the container, D is the gas diffusion coefficient, and $\bar{v}$ is the gas velocity in the tube averaged over the tube cross-section. For counter-current diffusion, $\bar{v}$ is negative. The use of the boundary conditon (7) ensures the maximum amount for diffusion, a conservative estimate.

By solving (5) for c we obtain the mass transfer rate $\dot{m}$ as

$$\dot{m} = \pi r^2 \left(\bar{v}c - D\frac{dc}{dz}\right) \tag{8}$$

and we define the fractional release rate f as

$$f = \dot{m}/c \tag{9}$$

The fractional release rate is

$$f = \begin{cases} \pi r^2 \bar{v}\dfrac{e^{\alpha}}{e^{\alpha}-1}, & \bar{v} <> 0; \\ \pi r^2 D/\ell, & \bar{v} = 0 \end{cases} \tag{10}$$

where $\alpha = \bar{v}\ell/D$.

2.2 RESULTS

Viscous Flow

We integrate (3) numerically to calculate the quantity n of gas inside a container and the gas flow rate in or out as functions of time. $\bar{T}$ and T_w have been obtained from *Site Characterization Plan*, [USDOE, 1988; p. 7-41] and extrapolated in time (Figure 3). We use a container thickness, ℓ, of 0.01 m. Argon viscosity is used when gas flows out, and air viscosity is used when air flows in. The results will be presented for two hole sizes, 5×10^{-6} meters (5 μm) and 10μm, and two fill temperatures, 298 K and 558 K. The fill pressure is assumed to be 0.1 MPa, and the hole is assumed to occur at emplacement or 300 years after the waste is buried. Figures 4 and 6 show the number of moles of gas inside the waste container as a function of time, and Figures 5 and 7 show the gas flow rate through the hole as a function of time.

In Figure 4 the dotted lines refer to outleakage and the solid lines refer to inleakage. For penetration at emplacement, a 5-μm hole, and a fill temperature of 298 K, argon slowly leaks out until about 800 years, after which leaking and repository cooling cause the internal pressure to fall below atmospheric, and air leaks in. For a 5-μm hole, 25% of the argon flows out, whereas for a 10-μm hole, 32% flows out. For a 10-μm hole, the internal pressure rapidly falls to atmospheric, and inleakage begins at about 70 years. For a 558 K fill temperature, the maximum gas temperature in waste packages, there is no thermally generated buildup

of pressure and thus no gradient for outleakage. Here a penetration results only in inleakage of air because the internal pressure is always less than atmospheric. Although not shown, inleakage curves for holes larger than 10-μm are nearly identical to the 10-μm curves. Thus, for these large holes, the quantity of gas within the container after inleakage begins depends only on the rate of cooling, independent of hole size.

Figure 5 shows the flow rate of gas in and out of the waste container for penetration at the time of maximum temperature after emplacement, the derivative of the curves in Figure 4. For a 558 K fill temperature, the pressure gradient and flow are zero at the time of penetration. As the waste cools, the rate of inleakage increases, reaches a maximum, and then decreases to a nearly constant rate that depends only on the cooling curve. Again, the slight upward slope at late times is because T_w in the denominator of (2) is decreasing with time.

Figures 6 shows the quantity of gas inside a waste container, and Figure 7 shows the flow rate of gas into and out of the waste container, both as functions of time, for the hole occurring at 300 years. The patterns are similar to the hole occurring at emplacement.

The results above are important in assessing containment performance, but we are interested here in radionuclide release rates. Figures 4 through 8 can be used to estimate release rates. In Figure 4 for a 298 K fill temperature and a 5-μm hole, about one-fourth of the gas and volatilized radionuclides leaks from the container. For 10-μm holes or larger, almost half of the gas leaks out before air inleakage begins.

We assume that $^{14}CO_2$ was released from the fuel cladding surface at the time of maximum temperature. It leaks out congruently with argon. We can then compute a $^{14}CO_2$ molar flow rate assuming no further volatilization of CO_2 during this period. The molar flow rate of $^{14}CO_2$ is the molar flow rate of argon from Figure 5, times the mole fraction of $^{14}CO_2$. Knowing the fraction of total ^{14}C inventory released quickly from the fuel cladding surface, we can compute the ^{14}C fractional release rate based on total inventory.

The fractional leak rate for other volatile species released initially to the container gas space is the ratio of the argon leak rate to the argon mass in the container times the volatile fraction of those species.

Assuming that heating of the waste package volatilizes 10 percent of the ^{14}C inventory [Park and Pflum 1990], primarily from cladding surfaces, a 5-μm hole and 298 K fill temperature result in an initial argon leak rate of 0.06 mole/a and a ^{14}C initial fractional leak rate of 2×10^{-5}/a. For a fill temperature of 558 K or higher, no radioactive material will be released if counter-diffusion is neglected.

Knudsen/Molecular Flow

To show the relative magnitudes of viscous flow and molecular flow, we calculate the flow rate of argon at 500 K through various aperture sizes, under identical pressure gradients (P = 0.19 MPa, P_0 = 0.1 MPa). The results are shown in Table III. Values in italics are for the flow regime that actually occurs. Other values are hypothetical.

Table III shows that molecular flow occurs in the smaller holes, but the actual flow rate and quantity of gas moving through the such small penetrations is miniscule and unimportant. For the 1-μm hole in Table III, the mean free path (Table II) is one tenth the hole radius, therefore viscous flow occurs. The actual penetration sizes that result in the overall single penetration considered here may be individually

small enough for Knudsen flow to occur. Assuming viscous flow through these larger equivalent single-hole penetrations is conservative.

If the actual penetrations are few in number and are near the size of the equivalent single holes considered here, the actual flow regime will be viscous, as has been analyzed. Even if the distribution of hole sizes includes many small holes in which Knudsen flow occurs, viscous flow through even a few larger holes is likely to dominate the leak rate. This is illustrated by the calculated results in Table III.

Table III. Comparison of Molecular and Viscous Flows of Argon for the Same Pressure Gradient, $T = 500$ K, $P = 1$ MPa, $P_0 = 0.1$ MPa, $\ell = 0.01$ m

Flow Rate (moles/a)		
Hole Diameter μm	Molecular	Viscous
0.01	1.6×10^{-10}	1.1×10^{-12}
0.1	1.6×10^{-7}	1.1×10^{-8}
1	10^{-4}	10^{-4}
10	10^{-1}	10
100	10^{2}	10^{4}

Diffusive Release

To calculate $^{14}CO_2$ release by combined advection and diffusion we combine the solution to the viscous flow model, (2) and (3), and the solution for diffusive release, (8). At each time-step we find the average viscous-flow velocity $\bar{v}$ and calculate the release rate using (8). Using a mass balance at each time step, we calculate c_0, the ^{14}C concentration inside the container in (6). Thus the depletion of ^{14}C in the container is accounted for.

Because counter-flow is a resistance to diffusion, assuming $\bar{v} = 0$ will give an upper bound to the counter-diffusion release rate. The upper curve in Figure 8 shows the diffusive fractional release rate as a function of penetration radius for D=0.27 cm^2/s, the diffusion coefficient for CO_2-air at 400 K. Multiplying these values by the fraction of the total radionuclide inventory that is volatilized, gives the inventory-based fractional release. For a 5-μm hole and 10 percent ^{14}C volatilized, the diffusive fractional release rate is 7×10^{-7} year^{-1} based on total ^{14}C inventory.

The lower curve in Figure 8 shows the fractional release with a molar flow rate of 5×10^{-3} moles/year, which is the late-time inflow rate for holes larger than 10-μm from Figure 5. This corresponds to a volumetric flow rate of 5×10^{-6} cm^3/s at 390 K. For holes smaller than 30-μm there is a reduction in the release rate, but for larger holes the flow is slow and diffusion is the dominant release mode.

2.3 C-14 RELEASE RATES

We now use the above analysis to derive ^{14}C release rates from a single waste package. For this calculation we use the following data

C-14 Release and Transport

Container gas volume, $V = 1.22$ m^3
Wall thickness, $\ell = 0.01$ m
External gas pressure, $P_0 = 0.1$ MPa
Internal gas fill pressure, $P = 0.1$ MPa
Internal gas fill temperature, 298 K
Internal gas temperature-time data from *Site Characterization Plan* [USDOE 1988; p. 7-41]
Initial ^{14}C inventory 3.1 Ci (1.1×10^{11} Bq) per package
Volatile ^{14}C fraction = 10% (assumed, after Park and Pflum [1990])
Diffusion coefficient of CO_2 in air = 0.27×10^{-4} m^2/s [Source: Bird, Stewart and Lightfoot 1960]

We calculate ^{14}C release rates shown in Figure 9 and 10, for holes of one to 300-μm occurring at emplacement and 300 years. In Figure 9, for a 1-μm hole, argon flows out for all time and carries with it $^{14}CO_2$. The initial release rate is 10^{-6} Ci/year (3.7×10^4 Bq/a) and decreases as the argon flow decreases. For a 5-μm hole, the initial $^{14}CO_2$ release rate is 5×10^{-4} Ci/year (1.9×10^7 Bq/a) and the release is mainly by advection. At about 900 years, air begins to flow into the container, and the release decreases sharply due to counter-diffusion resistance from air inflow. For a 10-μm hole, the initial release rate is almost 10^{-2} Ci/year (3.7×10^8 Bq/a). At about 70 years, air begins to flow into the container, and the release rate decreases sharply. As the cooling rate slows, the air inflow rate decreases and the counter-diffusion resistance decreases. Then the ^{14}C release rate reaches a near-constant rate.

For holes 20-μm or larger, the pressure inside the container falls rapidly near atmospheric when the hole occurs. About 50% of the argon and $^{14}CO_2$ is released immediately, after which air begins to flow into the container. The mass rate of air inflow is independent of the hole size and is determined solely by the cooling rate. However, the air velocity (and thus the resistance to diffusion) does depend on the hole size.

Thus, for all holes larger than 20-μm, 0.144 Ci (5.3×10^9 Bq) of ^{14}C is released at penetration, if the hole occurs at emplacement. The initial pulse is 0.097 Ci (3.6×10^9 Bq) for the hole occurring at 300 years.

For the 20-μm and 30-μm holes, the air inflow is a resistance to diffusion and the release rate after the initial pulse is low. As the air inflow rate decreases, the $^{14}CO_2$ release rate increases.

For the 100-μm, 200-μm, and 300-μm holes the air inflow velocity is so small that there is little, if any, resistance to the outward diffusion of $^{14}CO_2$. The slight increase in the release rate for the 100-μm hole is due to the decrease in the air inflow rate. The later decrease in the release rate for these three hole sizes is due to depletion of the $^{14}CO_2$ in the container.

For holes occurring at 300 years, the major difference is that for the larger holes only about 30% of the argon and $^{14}CO_2$ is released at penetration time because the waste container is cooler and the internal gas pressure is less than that emplacement. Thus the initial release pulse is 0.097 Ci (3.6×10^9 Bq) of ^{14}C.

This is our recommended release rate for far-field transport of ^{14}C, shown in Figure 11. Assume an initial release of 0.144 Ci/package (5.3×10^9 Bq/package) for a hole occurring at emplacement and 0.097 Ci/package (3.6×10^9 Bq/package) for a hole occurring at 300 years. From Figures 9 and 10, an upper bound for the time-dependent release rate of ^{14}C can be obtained by using the maximum release rate at each time. In both

Figures 9 and 10, the highest release rates after the initial pulse are for a 300-μm hole, except for a 10-μm hole where the flow rate decreases rapidly. We move down the release rate of the 300-μm hole to where it intersects the 200-μm hole in Figure 10, and move on in time until the 100-μm is intersected, forming an envelop of maximum release rates at all times. Clearly this will give a cumulative release greater than the assumed volatile fraction of ^{14}C, but this gives a conservative estimate.

In the Working Group 2 report on the Nominal Case, the waste packages in the repository are assumed to fail according to the fraction that can be wetted after the thermal period, and an repository-ensemble release rate calculated on the basis of a convolution between a single-waste-package release rate and the time-distribution of failures. Here we have not adopted such an approach because holes in waste containers resulting in gas-phase release can occur without the re-introduction of water into the immediate vicinity of waste packages. Indeed, the higher temperatures during the thermal period could increase corrosion rates and increase the probability of holes in waste containers.

3. FAR-FIELD TRANSPORT OF C-14

Using the time-dependent release rate just derived, we calculate the transport of ^{14}C from the proposed nuclear waste repository at Yucca Mountain using a porous-medium model. Use of this model is justified if the Peclet number is much less than unity, which indicates local equilibrium between gas in fractures and liquid in rock pores [Light *et al.* 1990]. We calculate $^{14}CO_2$ concentrations in soil gas, $^{14}CO_2$ fluxes and $^{14}CO_2$ concentrations when diluted by atmospheric dispersion. We also calculate cumulative release of ^{14}C into air from the ground surface and dose to a maximally exposed individual.

3.1 ANALYSIS

We assume that ^{14}C is released from failed waste canisters as $^{14}CO_2(g)$. Because CO_2 dissolves readily in water, we expect much of the ^{14}C to be retarded by absorption into vadose water. Some ^{14}C will react to form calcite and other minerals, but the fraction in solid phases is difficult to predict and probably not significant compared to the fraction in gas and liquid phases. We neglect precipitation into solid phases. However, we utilize the capacity of calcite to maintain a constant pH in vadose water.

The degree to which CO_2 dissolves in water is well known and the reaction rate is expected to be sufficiently fast in the time scales considered here to reach local chemical equilibrium. For $^{14}CO_2$, we adopt the equilibrium values for CO_2 in pure water at infinite dilution. Corrections for ^{12}C-^{14}C fractionation, capillary effects, and exact air and water compositions are expected to be small relative to other model uncertainties and are not included. The four aqueous species—CO_2, carbonic acid, and bicarbonate and carbonate ions—account for almost all of the liquid-phase carbon. Organic carbon is neglected. Using the equilibrium values for these species, a good approximation can be made of the equilibrium concentration ratios of $^{14}C(g)$ and $^{14}C(aq)$ in adjoining gas and liquid as a function only of temperature and pH.

We define the gas-liquid distribution coefficient for inorganic carbon to be

$$K_D = \frac{[H_2CO_3^*] + [HCO_3^-] + [CO_3^{2-}]}{[CO_2(g)]} \tag{11}$$

$[H_2CO_3^*]$ is a hypothetical species used to represent $[H_2CO_3]$ and $[CO_2(aq)]$. It can be shown that for most

natural waters [Snoeyink and Jenkins 1980]

$$[H_2CO_3^*] \cong [CO_2(aq)]$$

Depending on the pH and temperature, K_D may be as low as 2 or as high as 400 for expected repository conditions. We use $K_D = 3$, corresponding to 50 C and pH 7 [Stumm and Morgan 1981; Phillips, Phillips and Skeen 1985].

Fracture-Matrix Transport

The main purpose of the fracture model is to demonstrate that gas-phase carbon in fractures is at equilibrium at a given elevation z with liquid-phase carbon in the rock between the fractures. The tendency of the gas and liquid to equilibrate will be offset by the different flow velocities of the two phases and the physical separation between fractures and rock pores.

We consider a single vertical planar fracture filled with gas, adjacent to a porous medium, as shown in Figure 12. We neglect dispersion in the fracture and assume that the gas is well-mixed over the width of the fracture so that the concentration is uniform in the fracture in the y-direction. We also assume uniformity in the x-direction for concentrations in the fracture and rock matrix, and we assume a constant, upward gas velocity in the fracture.

We define a Peclet number as

$$\mathrm{Pe} \equiv \frac{b v_g}{\epsilon_g D_g + \epsilon_l D_l K_D} \tag{12}$$

where b is the fracture half width [L],
D_g is the pore-gas diffusion coefficient [L^2/t],
D_l is the liquid-phase diffusion coefficient [L^2/t],
v_g is the gas velocity in the fracture [L/t],
ϵ_g is the gas-filled porosity, and
ϵ_l is the liquid-filled porosity.

We conclude that if the Peclet number is much less than unity, the liquid concentrations in the rock matrix between fractures will be well equilibrated with gas concentrations in the fractures. For details of this analysis see Light *et al.* [1990].

Equivalent Porous Medium Transport

If there is equilibrium between ^{14}C in the fractures and in all rock-matrix pore liquid at a given z, we can treat the whole as an equivalent porous medium without regard to fracture details. Assuming local equilibrium, we replace $C_l(\mathbf{r},t)$ with $K_D C_g(\mathbf{r},t)$ in the general porous-medium governing equations and assume constant coefficients, yielding

$$\left(\frac{\partial}{\partial t} + \lambda\right) C_g(\mathbf{r},t) + \mathbf{v} \cdot \nabla C_g(\mathbf{r},t) - D\nabla^2 C_g(\mathbf{r},t) = \frac{f(\mathbf{r},t)}{\epsilon_g + \epsilon_l K_D} \tag{13}$$

where

$$\mathbf{v} = \frac{\mathbf{q}_g + \mathbf{q}_l K_D}{\epsilon_g + \epsilon_l K_D}, \quad D = \frac{\epsilon_g D_g + \epsilon_l D_l K_D}{\epsilon_g + \epsilon_l K_D} \tag{14}$$

Here $\mathbf{q}_g$ is the gas Darcy velocity, $\mathbf{q}_l$ is the liquid Darcy velocity, and $f(\mathbf{r},t)$ is a source term. The scalar diffusion coefficients D_g and D_l have been used in place of dispersion tensors.

Solutions to (13) are well known for various source terms, boundary conditions and initial conditions. We assume an infinite domain with the concentration equal to zero initially and vanishing at infinity for all time. This assumption does not allow for a boundary condition at the ground surface. In reality, the ^{14}C gas concentration at the ground surface is near zero because of atmospheric dispersion. Therefore, the ^{14}C flux may be somewhat greater than predicted here due to the increased concentration gradient at the ground surface.

We consider solutions of both a single waste package as a point source and the entire repository as an infinite plane source for the time-dependent ^{14}C release rates in Section 2.3. For a point source with an impulse release the mathematical source term can be written

$$f(\mathbf{r},t) = I_f \delta(\mathbf{r})\delta(t-t_f) \tag{15}$$

where I_f is the amount of ^{14}C in the impulse release and t_f is the time of penetration. The solution for the point-source is

$$C_g(\mathbf{r},t) = I_f \frac{\exp\left[-\frac{(\mathbf{r}-\mathbf{v}(t-t_f))^2}{4D(t-t_f)} - \lambda(t-t_f)\right]}{(\epsilon_g + \epsilon_l K_D)[4\pi D(t-t_f)]^{3/2}}, \quad t > 0 \tag{16}$$

For an infinite plane source term with an impulse release

$$f(\mathbf{r},t) = \frac{I_f}{A}\delta(z)\delta(t-t_f) \tag{17}$$

where A is the area normal to z over which the release occurs. Similarly, the solution for the infinite-plane-source is

$$C_g(z,t) = \frac{I_f}{A} \frac{\exp\left[-\frac{(z-v(t-t_f))^2}{4D(t-t_f)} - \lambda(t-t_f)\right]}{(\epsilon_g + \epsilon_l K_D)[4\pi D(t-t_f)]^{1/2}}, \quad t > 0 \tag{18}$$

The flux from an infinite plane source with an impulse release is

$$\Phi(z,t) = \frac{I_f}{A} \frac{\exp\left[-\frac{(z-v(t-t_f))^2}{4D(t-t_f)} - \lambda(t-t_f)\right]}{[4\pi D(t-t_f)]^{1/2}} \left[\frac{z+v(t-t_f)}{2(t-t_f)}\right], \quad t > 0 \tag{19}$$

For the time-dependent release rates shown in Figure 11, the concentrations and fluxes have been calculated by the superposition of a series of impulses at 8 to 10 year intervals. To obtain a source strength for the repository-equivalent plane source, the time-dependent release rates shown in Figure 11 for a single container (3.1 Ci/package, 1.1 $\times 10^{11}$ Bq/package) have been multiplied by

$$\frac{\text{100000 Ci of C} - \text{14 in repository}}{\text{3.1 Ci/package}}$$

The above-ground $^{14}CO_2$ concentration c [Ci or Bq/L^3] is estimated by a method after Schiager [1974] for estimating exposures from a diffuse underground source

$$c = \frac{\Phi L}{\sigma_z U} \tag{20}$$

where L is the lateral extent of the repository [L],
U is the mean wind speed [L/t], and
σ_z is the vertical standard deviation of the assumed Gaussian distribution of concentration [L].

To convert above-ground $^{14}CO_2$ concentration to dose, we use the dose factor

$$10^8 \quad \frac{\text{mrem/a}}{\text{Ci/m}^3} \tag{21}$$

from a recent NCRP method [1989].

3.2 RESULTS

Release of $^{14}CO_2$ from waste in the proposed repository at Yucca Mountain is most likely during the thermal period when waste temperatures are high. Also associated with the thermal period are large thermally-driven gas velocities. One estimate for the gas velocity in fractures due to repository heating is 22 m/a (0.04 m/a Darcy velocity) [Tsang and Pruess 1987]. We assume zero liquid velocity. Other parameters include $\epsilon_g = 0.02$, $\epsilon_l = 0.08$, $K_D = 3$, $D_g = 50\,\text{m}^2/\text{a}$, and $D_l = 3 \times 10^{-3}\,\text{m}^2/\text{a}$. The diffusion parameters are based on measured values for molecular diffusion in gas [Green and Evans 1987] and liquid continuums and include ten-fold reductions due to tortuosity. They are without the presumably small corrections for hydrodynamic dispersion. The value for the fracture half-width, 10^{-5} m, is characteristic of reported values [Peters *et al.* 1984]. The half-life of ^{14}C is 5730 years.

The Peclet number is approximately 2×10^{-4}. This indicates that ^{14}C in pore liquid at fracture surfaces will spread quickly into the rock matrix between fractures. Thus ^{14}C in the gas will be retarded in accord with the local-equilibria assumption used in the equivalent-porous-medium model.

Retardation by the liquid phase is incorporated in the advective transport velocity $\mathbf{v}$ given by (14). This yields the speed that a ^{14}C plume would travel independent of dispersion. For the given set of values, $\mathbf{v}$ is about 0.015 m/a, suggesting 2300 years for ^{14}C to travel 350 m from the repository to the ground surface. However, dispersion will cause the plume to spread, and the leading edge will arrive at the ground surface more quickly.

To estimate above-ground $^{14}CO_2$ concentrations, the following values are used in (20). An atmospheric turbulence class of F, moderately stable conditions, has been assumed [Barr and Clements 1984].
$L = 3000$ m
$\sigma_z = 20$ m
Currently no site-specific wind speeds are available for Yucca Mountain. In the *Site Characterization Plan*, surface winds at Yucca Mountain have been estimated using historical wind data from four meteorological towers at Yucca Flat at the Nevada Test Site [p. 5-21]. Wind speeds are generally less than 5.4 m/s and 13.1 % of the time it is calm. Therefore we conservatively use
$U = 1$ m/s

Figure 13 shows the gas-phase concentration of ^{14}C as a function of distance above a single failed container if the hole occurred at emplacement, for the release rates adopted in Section 2.3. Note that the results are for a saturation of 0.8. For a gas Darcy velocity of 0.4 m/a, the peak concentration occurs at 200 to 300 years

and by 1000 years, much of the ^{14}C has reached the surface (350 m), demonstrating the effect of dispersion on travel time.

The maximum concentration in the plume decreases significantly as the plume spreads. This results almost entirely from gas-phase dispersion because little decay occurs in 1500 years. We conclude therefore, that dispersion has an important effect on both the travel time and the concentration at the ground surface for this data set.

Figure 14 shows the gas-phase concentration of ^{14}C as a function of distance above a single failed container if the hole occurred at 300 years, for the conditions discussed above in Section 2.3 C-14 RELEASE RATE. The peak concentration occurs at about 500 years and by 1200 years, much of the ^{14}C has reached the surface. Note also that the delay in failure has little effect on the peak concentration. For holes that occur at a latter time, the concentration profile decreases with gas Darcy velocity.

Figure 15 shows $^{14}CO_2$ flux at a point 350 m above the repository if a hole occurs in all containers in the repository at 300 years. The parameters in Figure 15 are the gas Darcy velocity and water saturation. Here and in all subsequent figures the repository has been treated as an infinite plane source, but with a planar area of 7×10^6 m^2. It can be seen that saturation has a larger effect on $^{14}CO_2$ flux when the gas Darcy velocity is lower.

Figure 16 shows $^{14}CO_2$ annual releases at a point 350 m above the repository if a hole occurs in all containers in the repository at 0 or 300 years, with gas Darcy velocity as a parameter. Water saturation is taken to be 0.8. The y-axis on the right shows the dose to a maximally exposed individual from air immersion, ground surface exposure and inhalation, calculated using the method discussed above in (20) to (21). The dose to that individual is very low, approximately 0.1% of background, for the peak release at a gas Darcy velocity of 0.4 m/a. This is from some extreme assumptions about container integrity.

Figure 17 shows $^{14}CO_2$ flux at a point 350 m above the repository if a hole occurs in all containers in the repository at 0 or 300 years, for a tuff saturation of 0.8. The parameters in Figure 17 are the gas Darcy velocity. The y-axis on the right shows the dose to a maximally exposed individual, calculated using the method discussed above in (20) to (21). Figure 18 shows cumulative releases of ^{14}C as a function of time of hole occurrence and gas Darcy velocity. The difference in steady-state cumulative releases due to different gas Darcy velocity is attributable to decay. The difference in cumulative amounts of the hole occurring at 0 year and 300 years is because we use a slightly different release rate for far-field transport, as discussed in Section 2.3 and Figure 11. It is interesting to note that if the gas Darcy velocity is as high as 0.4 m/a, then practically all of the ^{14}C released reaches the ground surface within several hundred years. If the gas Darcy velocity is 0.04 m/a, then it will take several thousand years, but well short of one half-life of ^{14}C, for all the released ^{14}C to reach the ground surface.

4. CONCLUSIONS

The release of ^{14}C as $^{14}CO_2$ from partly failed spent fuel containers has been analyzed by the flow of gases into and out of the containers. This flow of gases is driven by pressure differences, which are in turn caused by heating by the spent fuel. In this analysis, the timing and size of holes in the containers are assumed to be given. A better means of predicting the time distribution and sizes of penetrations in nuclear waste

containers is needed. For the purposes of far-field transport calculations, we have adopted release rates that are shown to be bounding for the large range of hole sizes studied.

The transport of released $^{14}CO_2$ has been analyzed by transport in equivalent porous medium. The peak $^{14}CO_2$ concentration in pore gas at 350 m above the repository does not depend on the time of hole occurrence, although the time of penetration obviously affects the arrival and duration of exposure to ^{14}C. Nor does water saturation have much effect on peak concentration. In earlier studies we have shown that the peak concentration is insensitive to release rate from the failed container, for a wide range of release rates.

Gas Darcy velocity is the most important parameter affecting $^{14}CO_2$ transport. It is difficult to calculate gas flow velocities in unsaturated rock, due to transient heating, bouyancy-driven flow, and the possibility of heat pipe effects. Thus, there is a high degree of uncertainly associated with this important parameter. In this analysis we have used a constant gas Darcy velocity. We performed limited sensitivity analysis on gas Darcy velocity by using values one order of magnitude above and below the published value. This probably gives us bounds on the likely gas Darcy velocity.

The retardation of $^{14}CO_2$ transport is due to absorption in vadose water, represented in our analysis by a K_D. Elsewhere we have shown the sensitivity of K_D to changes in pH and temperature although in the current analysis we use a constant value. It is not known what will be the pH and temperature variations at Yucca Mountain in response to waste emplacement, and this information is needed.

Our calculations, using the particular data set, show that essentially all the released ^{14}C will reach the ground surface in less than one half-life of ^{14}C. However, the quantities of ^{14}C reaching the ground surface are so small that even if all containers fail at emplacement and conservative dose factors are used, the resultant inhalation dose to the maximally exposed individual is about 0.1% of natural background radiation.

ACKNOWLEDGEMENT

This work was supported by the U.S. Department of Energy under contract DE-AC03-76SF00098.

REFERENCES

S. Barr and W. E. Clements, "Diffusion Modeling: Principles of Application," in D. Randerson (ed.), *Atmospheric Science and Power Production,* DOE/TIC-27601, 584, 1984.

R. B. Bird, W. E. Stewart, E. N. Lightfoot, *Transport Phenomena*, Wiley, New York 1960.

R. T. Green and D. D. Evans, Radionuclide Transport as Vapor Through Unsaturated Fractured Rock, *NUREG/CR-4654*, University of Arizona, 1987.

E. H. Kennard, *Kinetic Theory of Gases,* McGraw-Hill, New York 1938.

W. B. Light, T. H. Pigford, P. L. Chambré and W. W.-L. Lee, "^{14}C Transport in a Partially Saturated, Fractured, Porous Medium," Paper to appear in Scientific Basis for Nuclear Waste Management XIII, LBL-27199, 1989.

National Council on Radiation Protection and Measurements, "Screening Techniques for Determining Com-

pliance with Environmental Standards: Releases of Radionuclides to the Atmosphere," *NCRP Commentary 3,* 1989.

R. R. Peters, E. A. Klavetter, I. J. Hall, S. C. Blair, P. R. Heller, and G. W. Gee, Fracture and Matrix Hydrologic Characteristics of Tuffaceous Materials from Yucca Mountain, Nye Country, Nevada, *SAND84-1471,* Sandia National Laboratories, 1984.

K. J. Schiager, "Analysis of Radiation Exposure On or Near Uranium Mill Tailings Piles," *Radiation Data and Rpts, 15,* 411, 1974.

U. S. Park and C. G. Pflum, "Requirements for Controlling a Repository's Releases of Carbon-14 Dioxide; The High Costs and Negligible Benefits," Proceedings of the 1990 International High Level Waste Management Conference, Las Vegas, NV, 1158.

S. L. Phillips, C. A. Phillips and J. Skeen, Hydrolysis, Formation and Ionization Constants at 25 C, and at High Temperature-High Ionic Strength, *LBL-14996,* Lawrence Berkeley Laboratory, 1985.

V. L. Snoeyink and D. Jenkins, *Water Chemistry,* Wiley, New York, 1980.

W. Stumm and J. J. Morgan, *Aquatic Chemistry,* 2nd Ed. Wiley, New York, 1981.

Y. W. Tsang and K. Pruess, "A Study of Thermally Induced Convection Near a High-Level Nuclear Waste Repository in Partially Saturated Fractured Tuff," *Water Resources Res. 23,* 1958 1987.

U.S. Department of Energy, "Site Characterization Plan, Yucca Mountain Site, Nevada Research and Development Area, Nevada," *DOE/RW-0199* 1988.

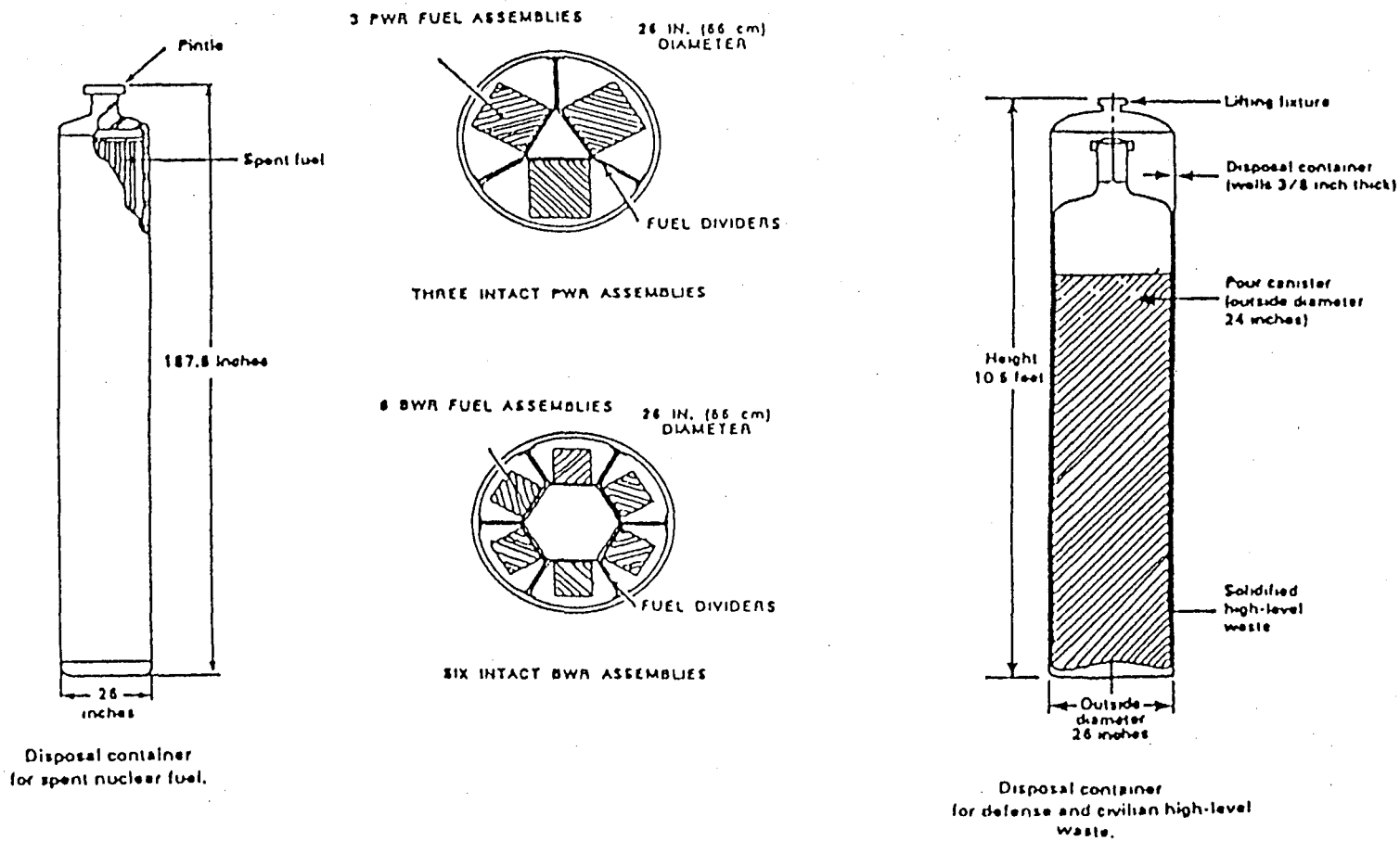

Figure 1. Typical Waste Packages

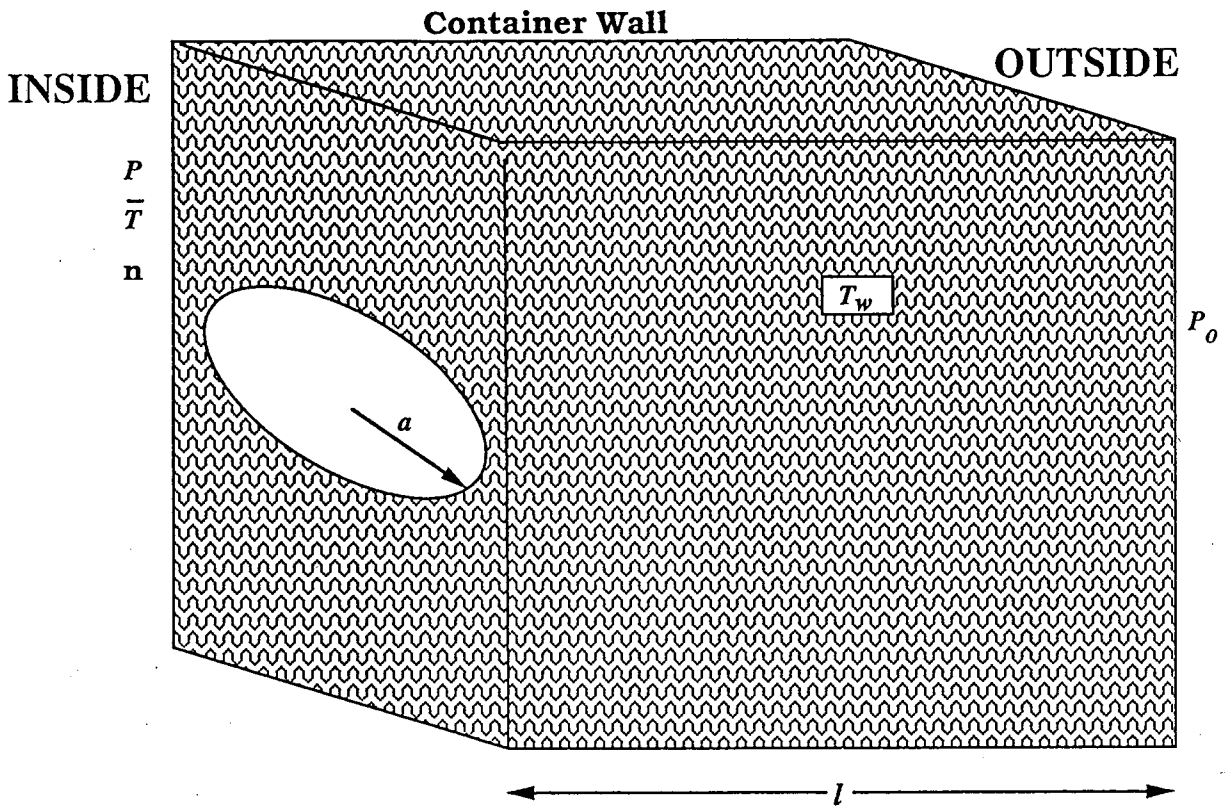

Figure 2. Penetration in a Container Wall

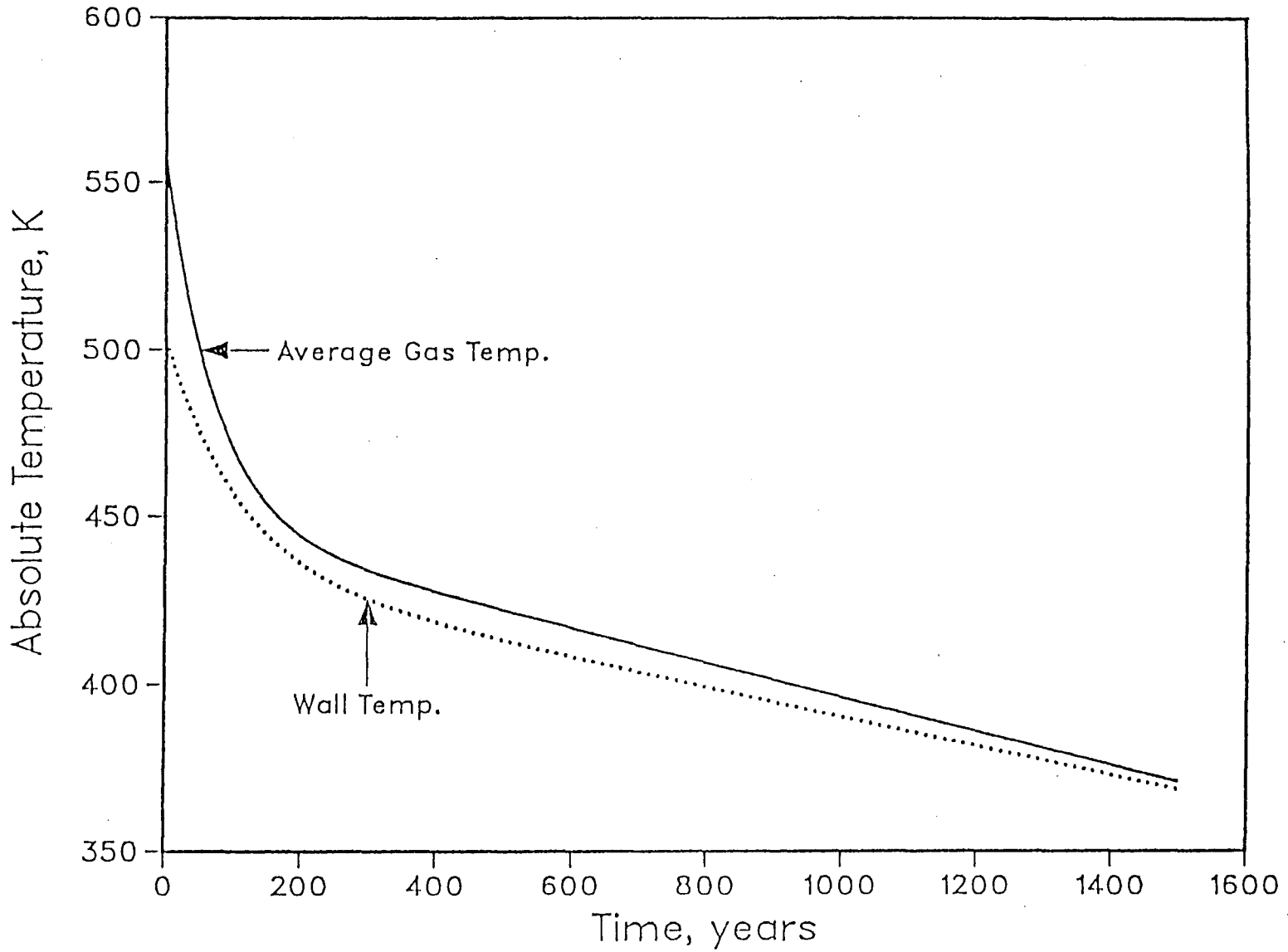

Figure 3. Waste Package Gas and Wall Temperature

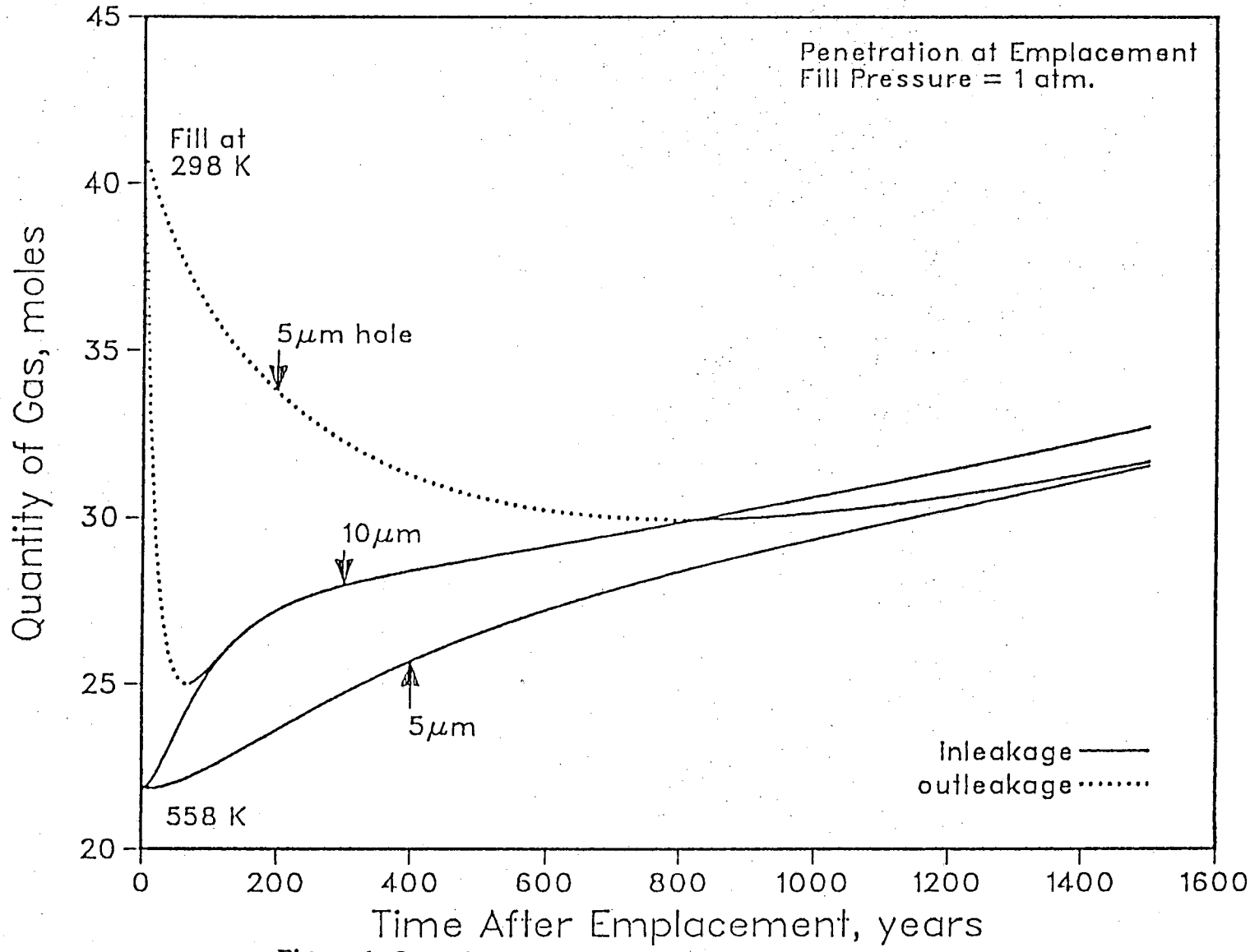

Figure 4. Quantity of Gas in a Container, Hole at Emplacement

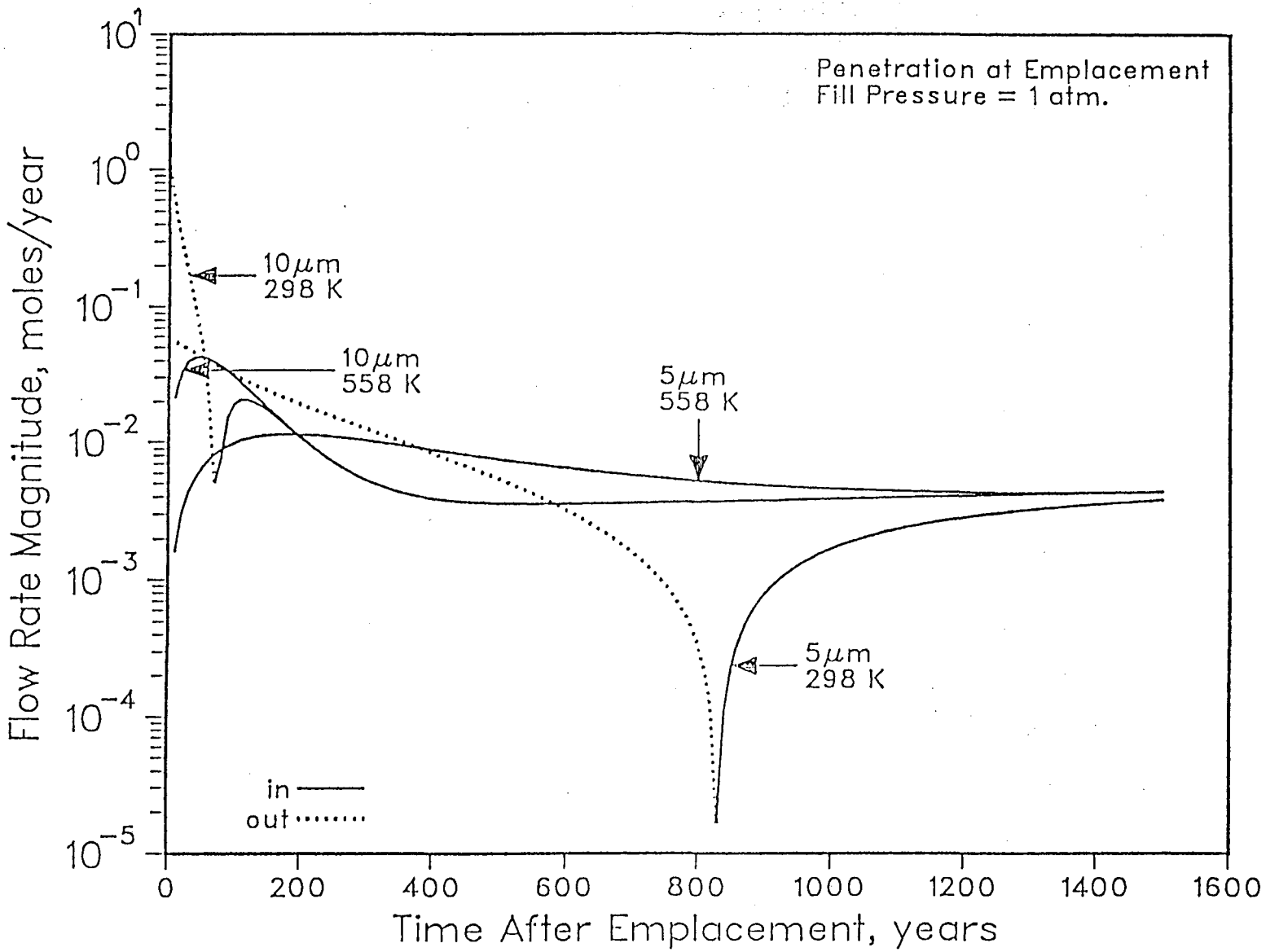

Figure 5. Gas Flow Rate, Hole at Emplacement

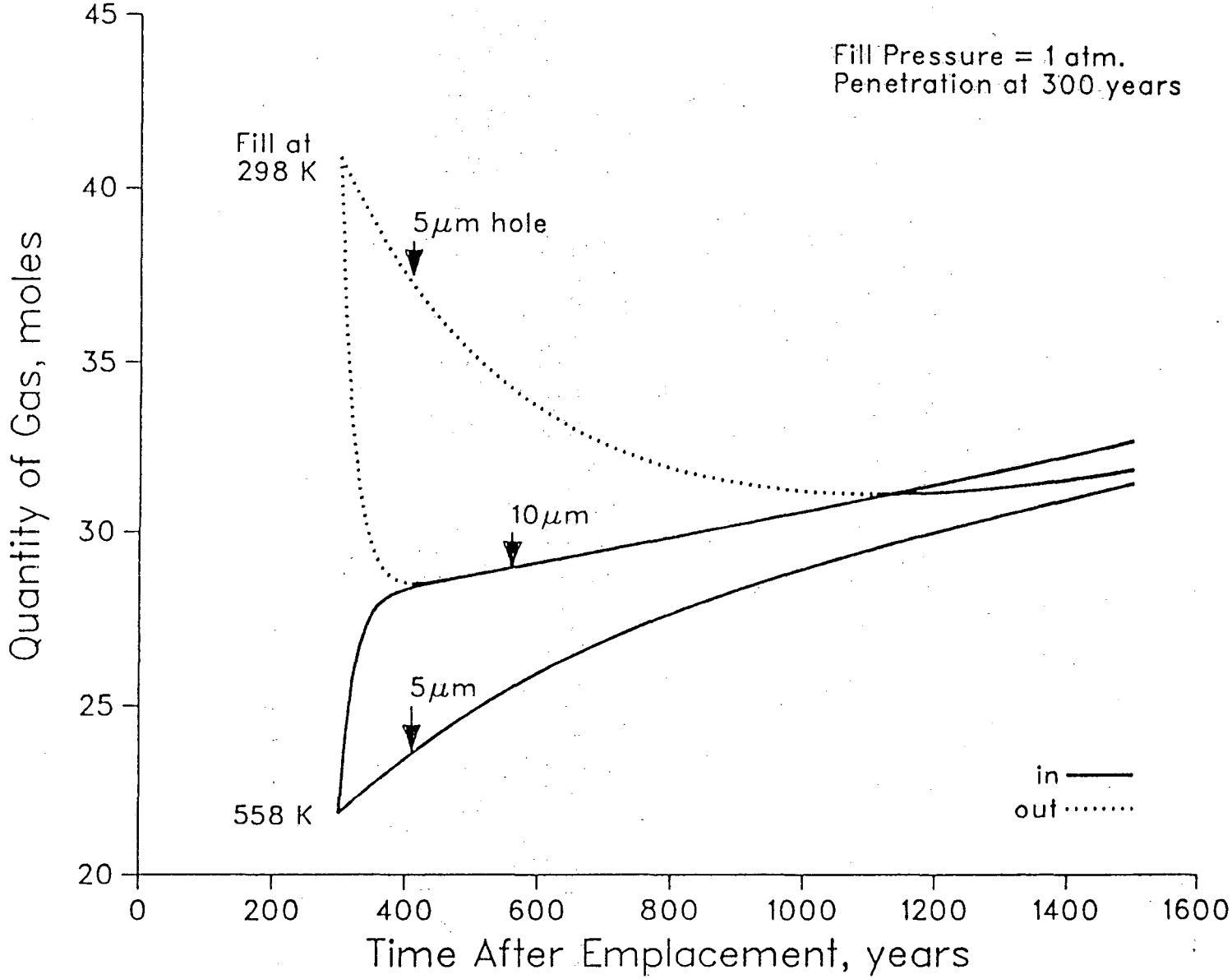

Figure 6. Quantity of Gas in a Container, Hole at 300 Years

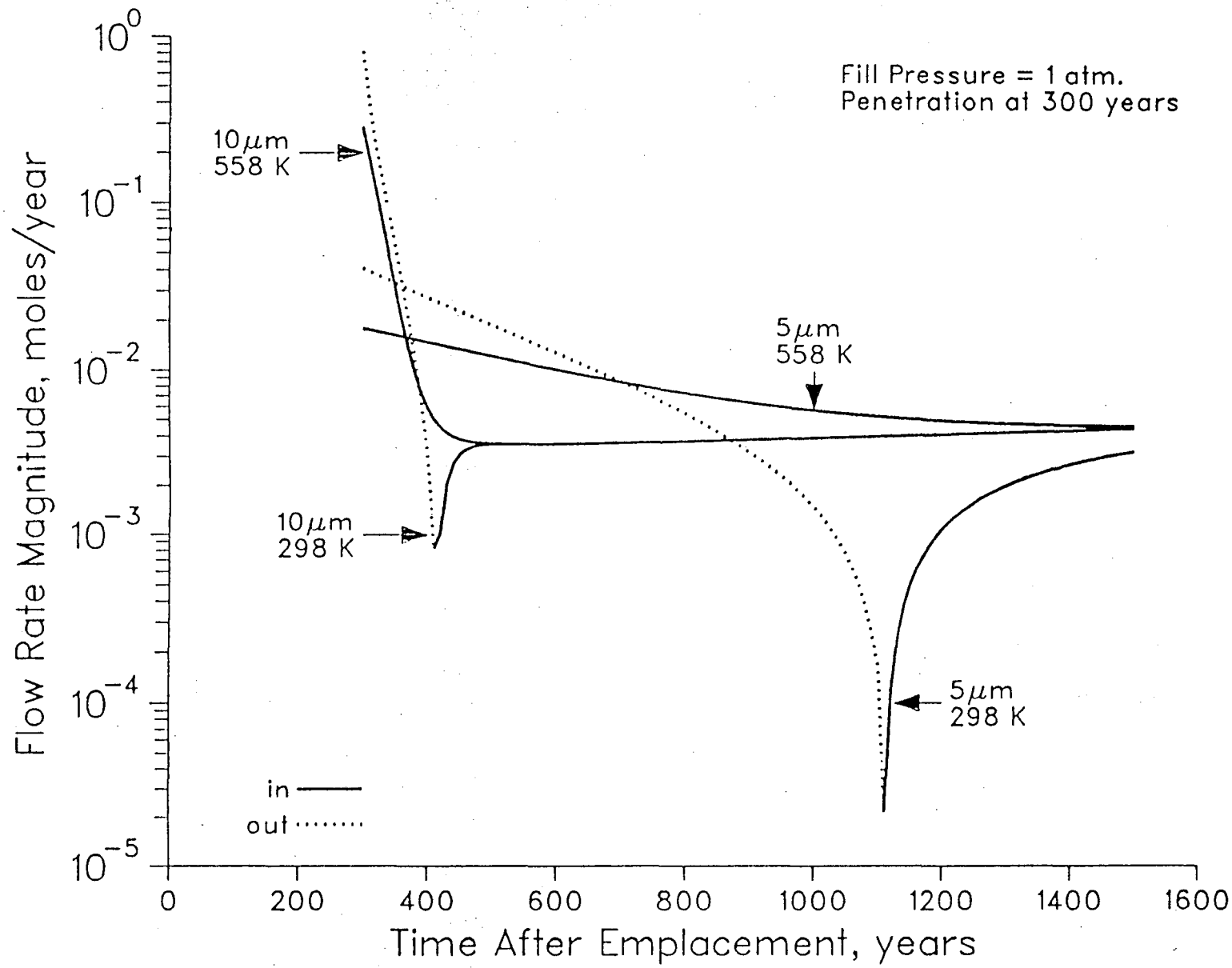

Figure 7. Gas Flow Rate, Hole at 300 Years

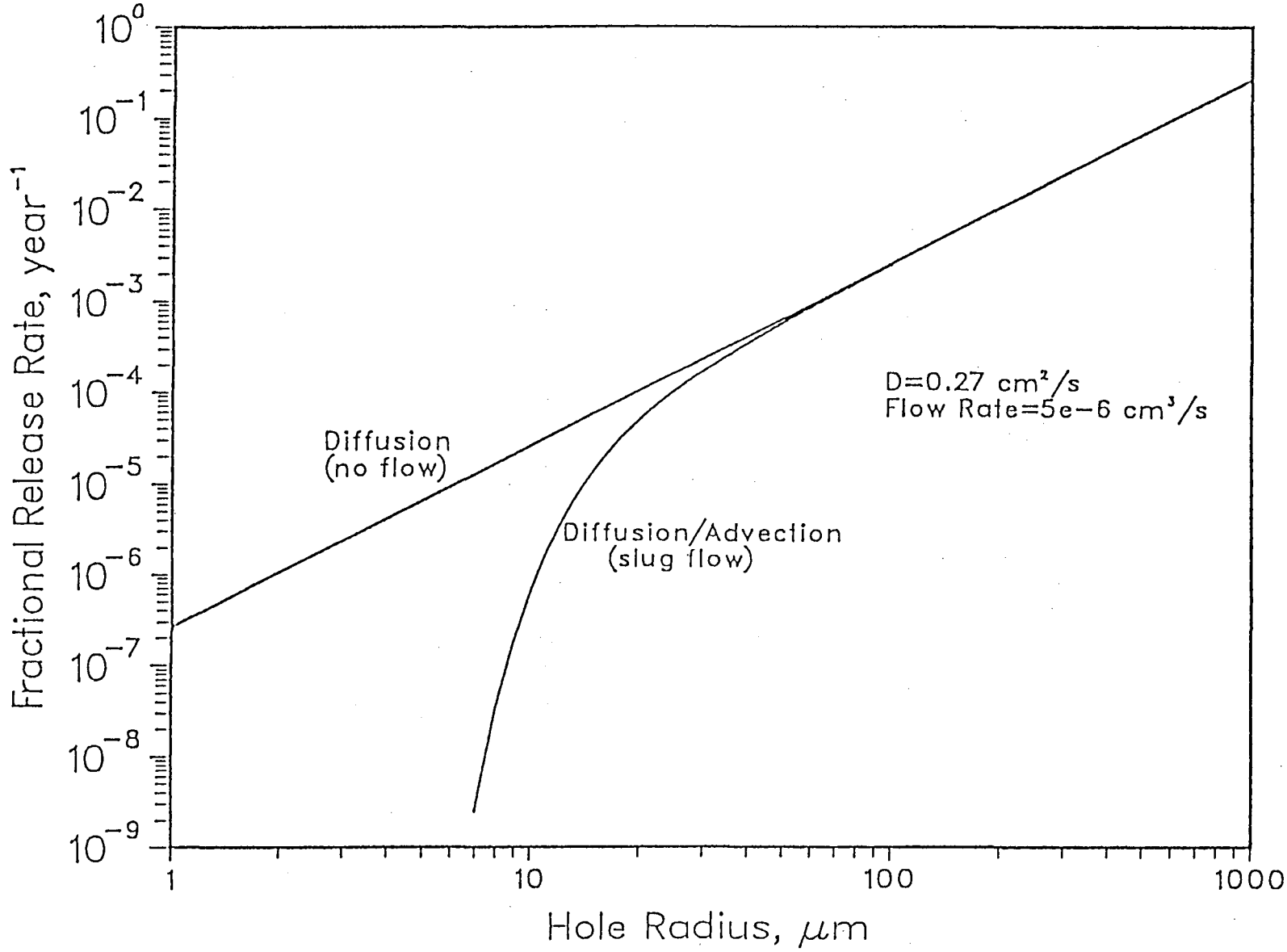

Figure 8. Fractional Release Rate with Slug Flow and Binary Diffusion

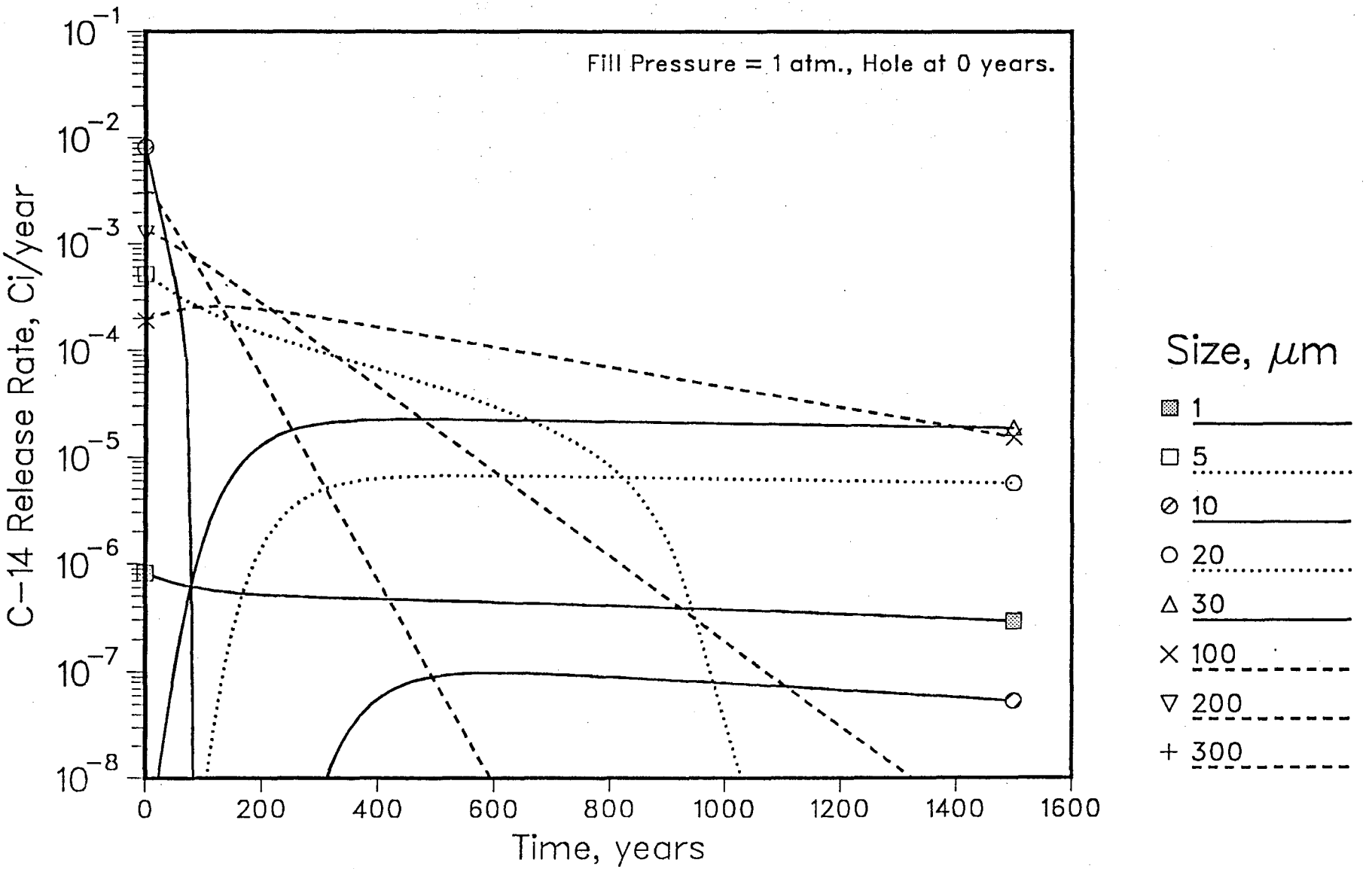

Figure 9. C-14 Release Rates for Various Size Holes Occurring at Emplacement

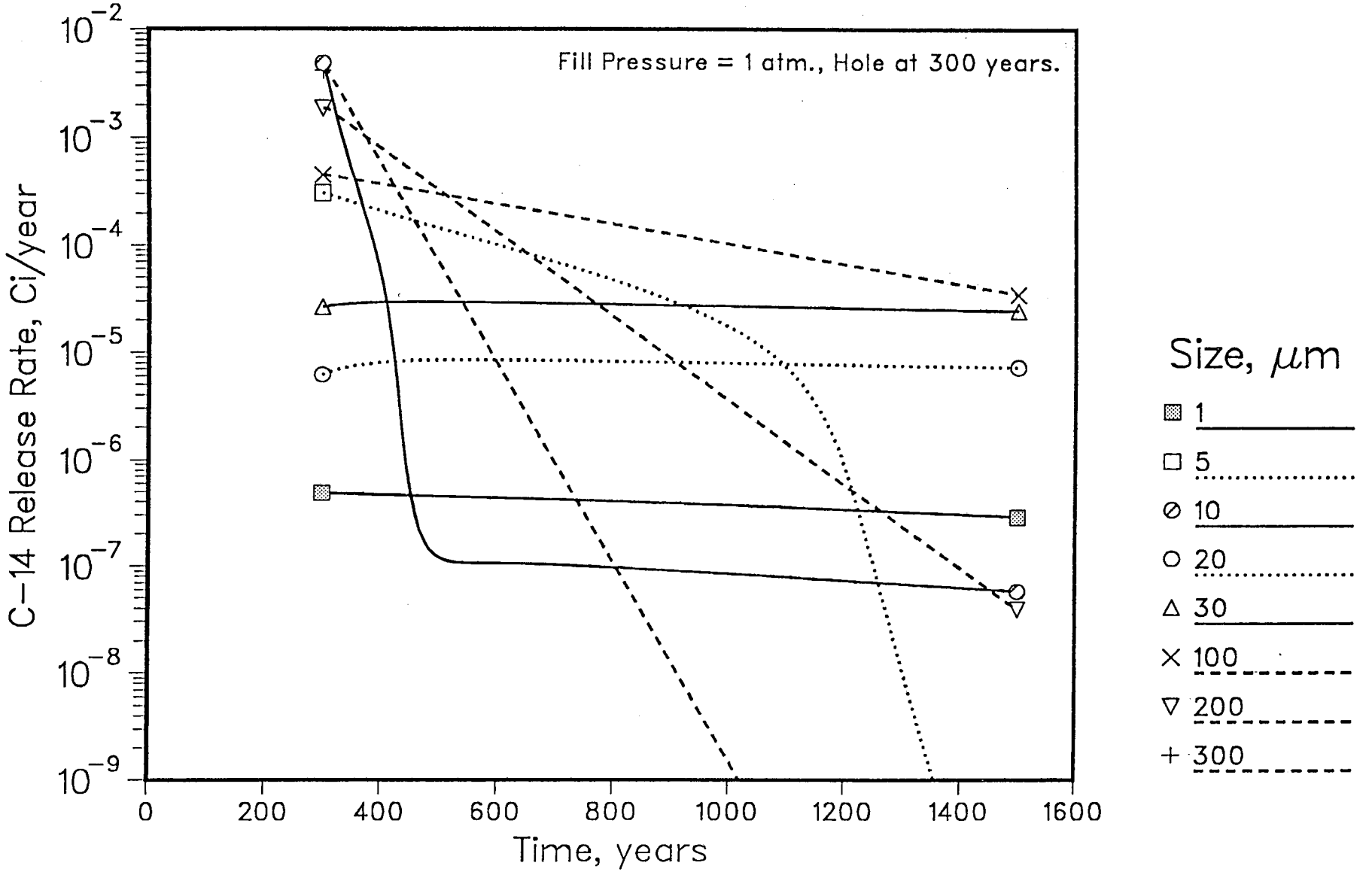

Figure 10. C-14 Release Rates for Various Size Holes Occurring at 300 Years

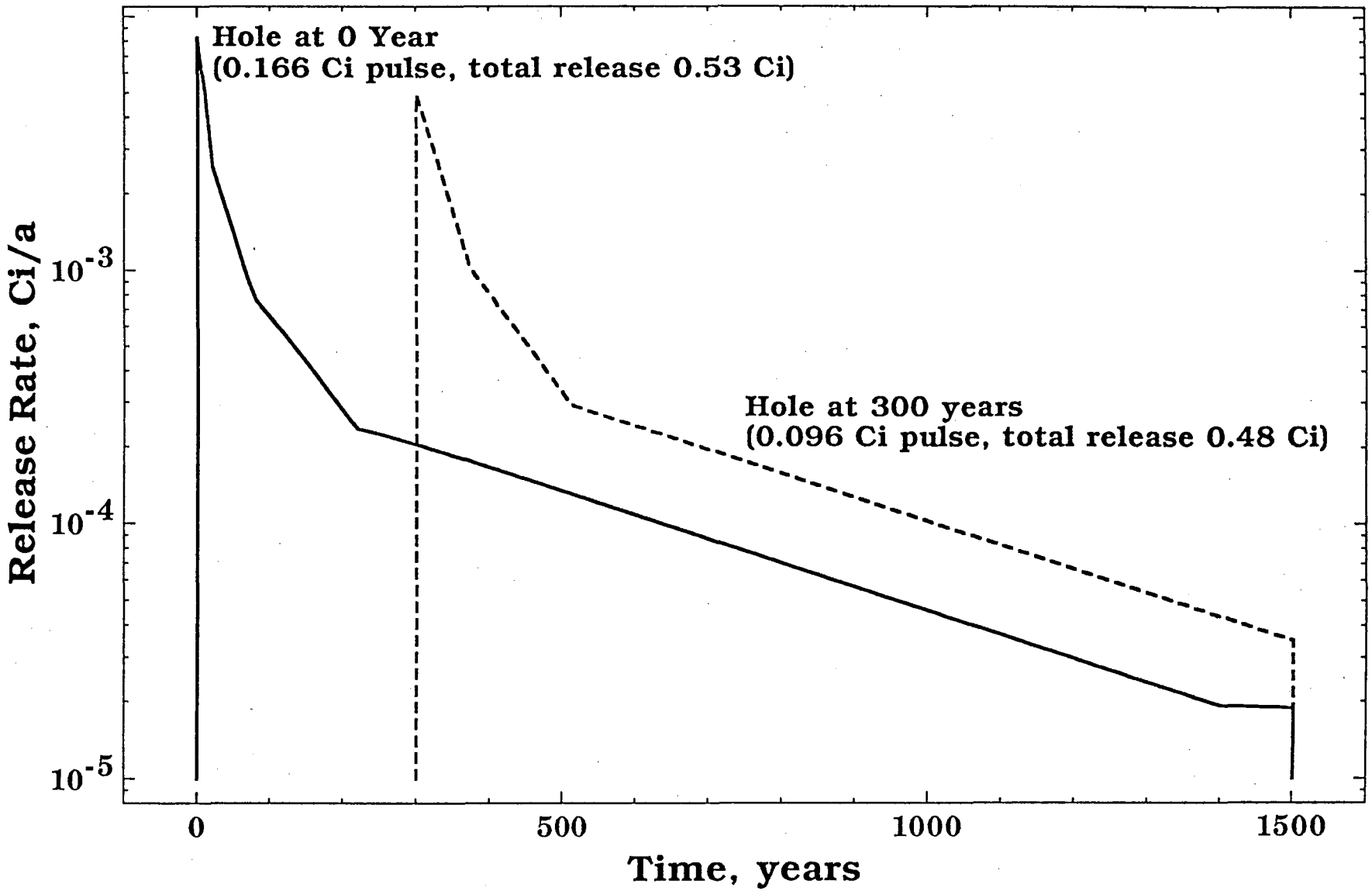

Figure 11. Composite C-14 Release Rates for Holes at 0 and 300 Years

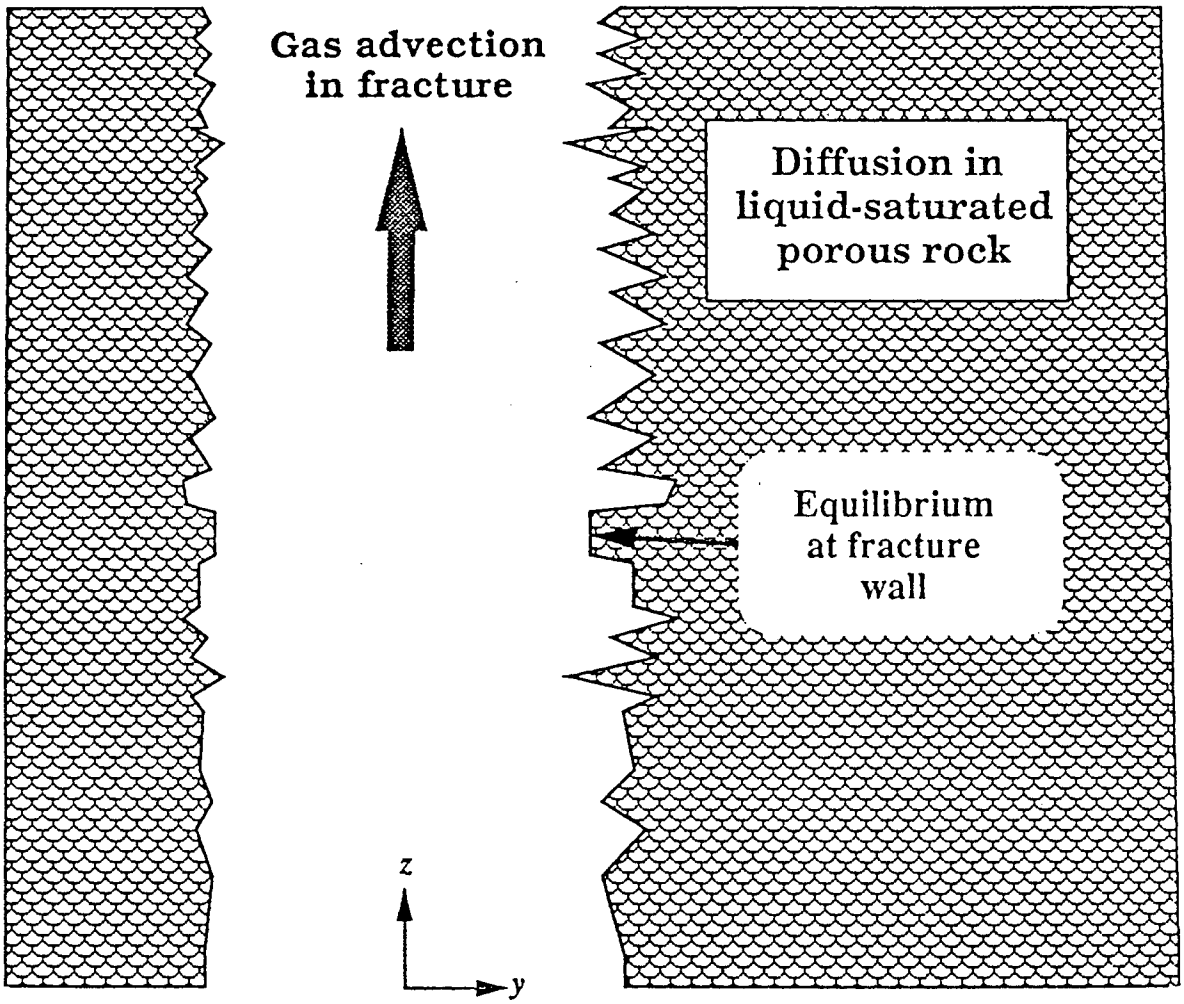

Figure 12. Gas Movement in a Fractured Porous Medium

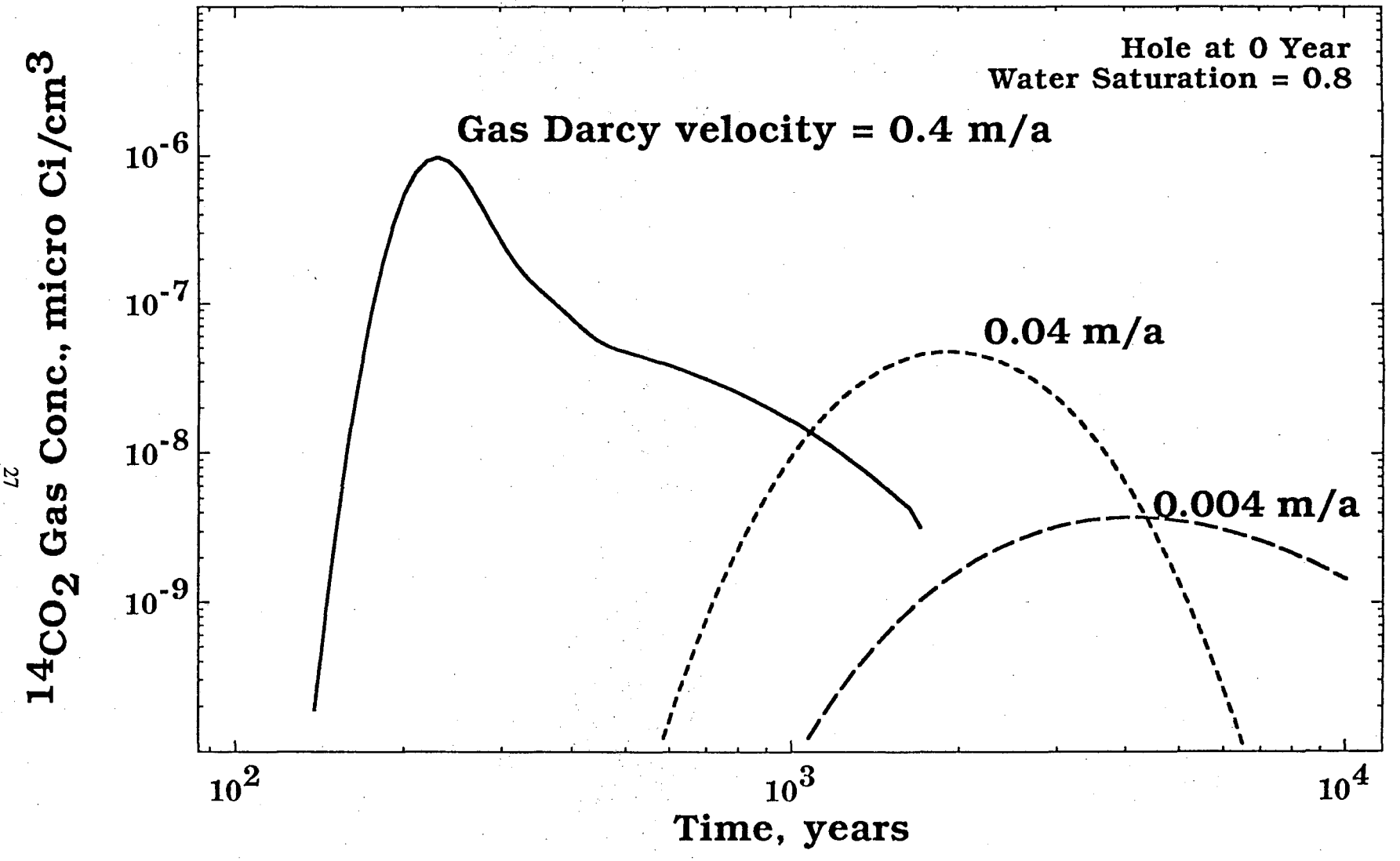

Figure 13. C-14 in Pore Gas 350 m Above a Repository, Hole at 0 Year in a Single Container

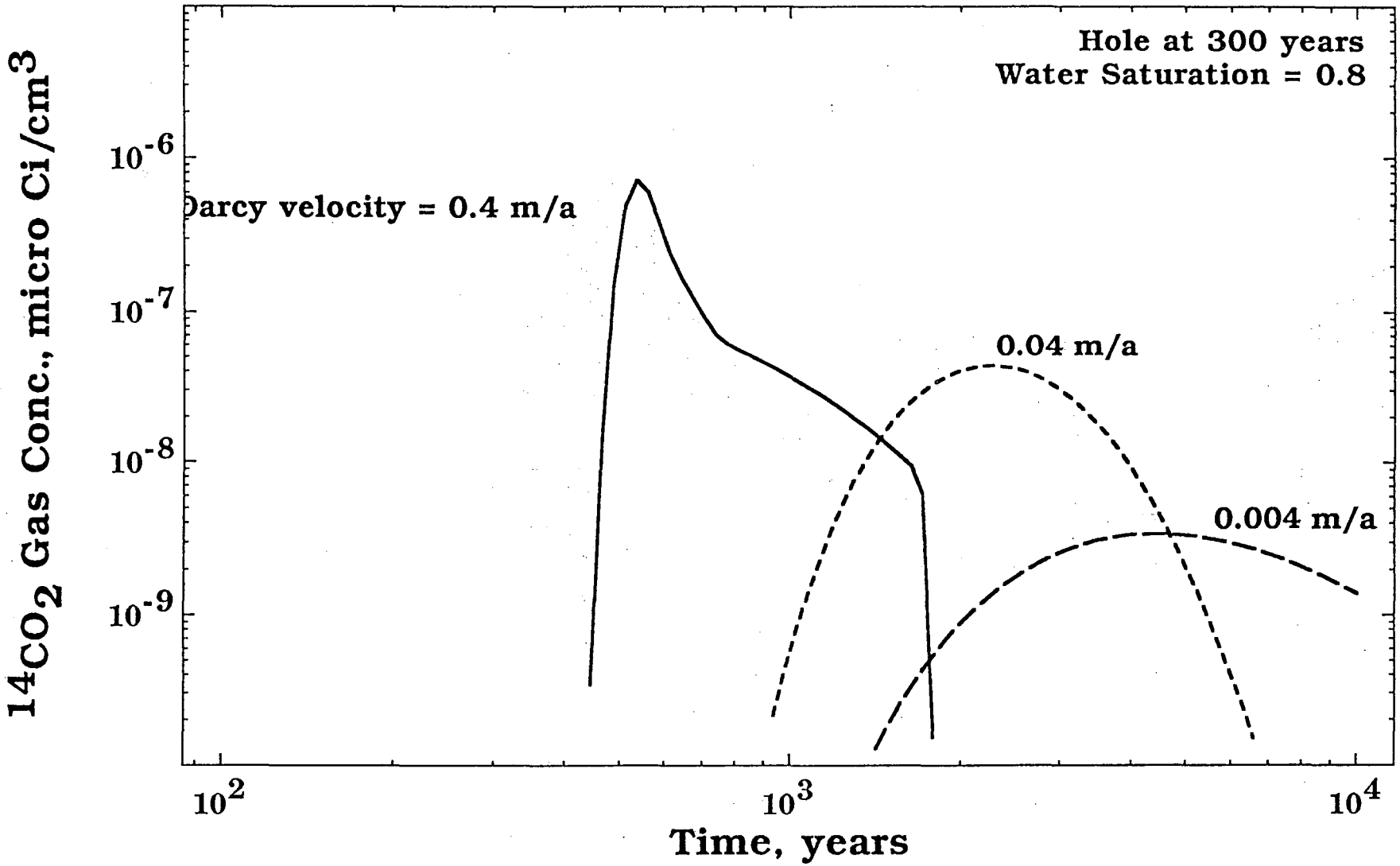

Figure 14. C-14 in Pore Gas 350 m Above a Repository, Hole at 300 Years in a Single Container

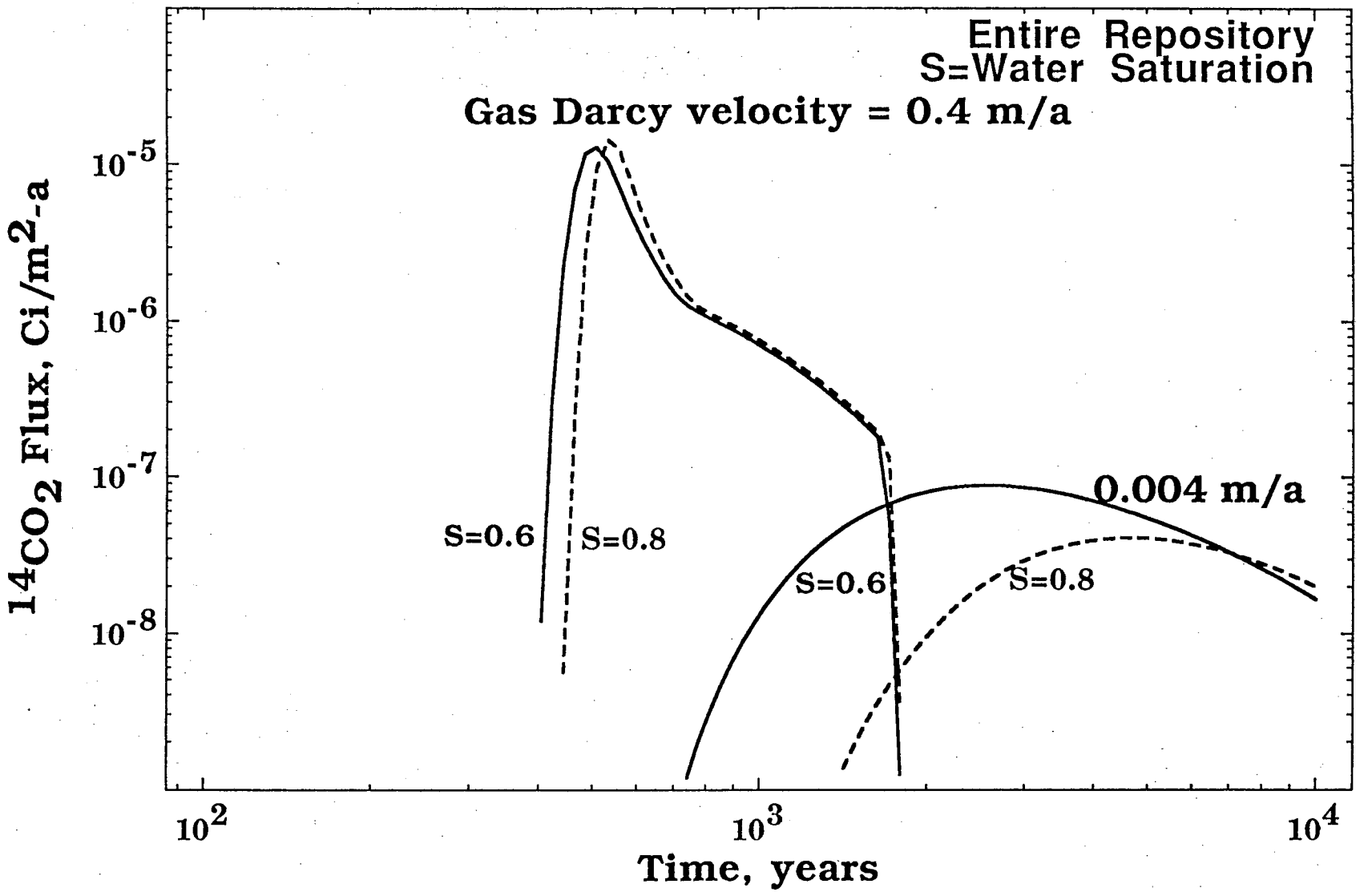

Figure 15. C-14 Flux at Ground Surface, Hole at 300 Years, Effect of Saturation

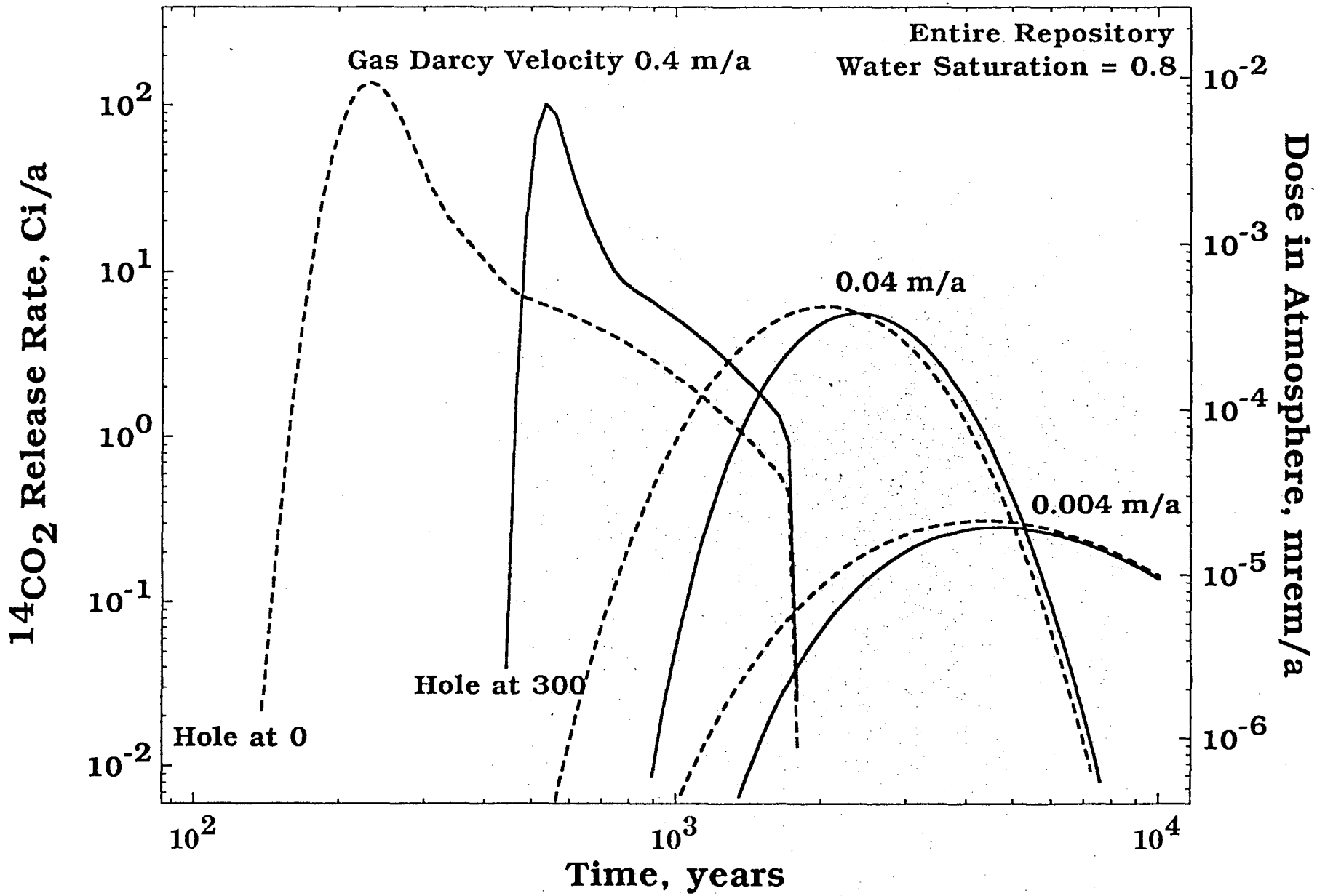

Figure 16. Annual Release and Dose of C-14 at Ground Surface, Hole at 0 or 300 Years

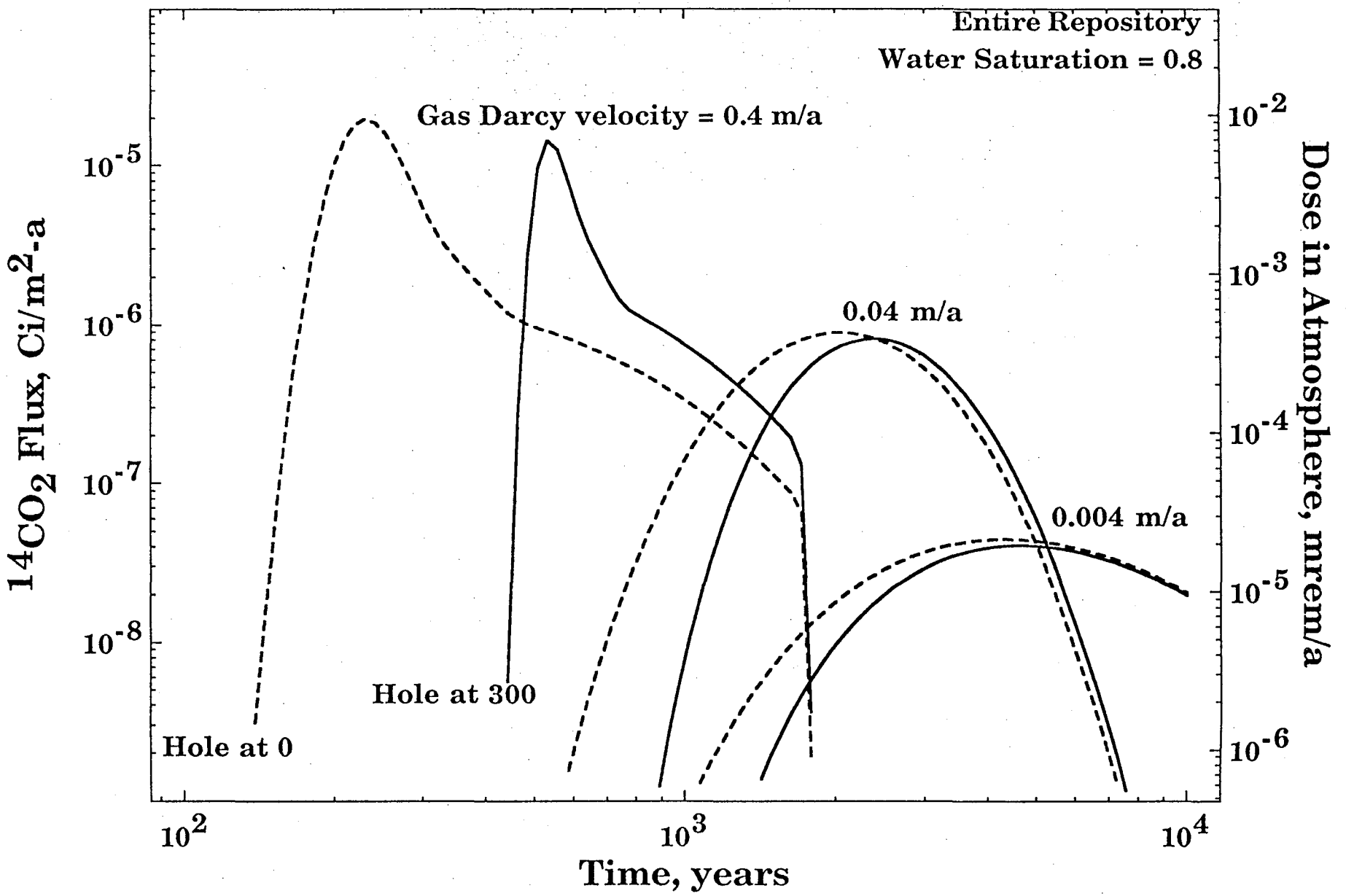

Figure 17. Flux and Dose of C-14 at Ground Surface, Hole at 0 or 300 Years

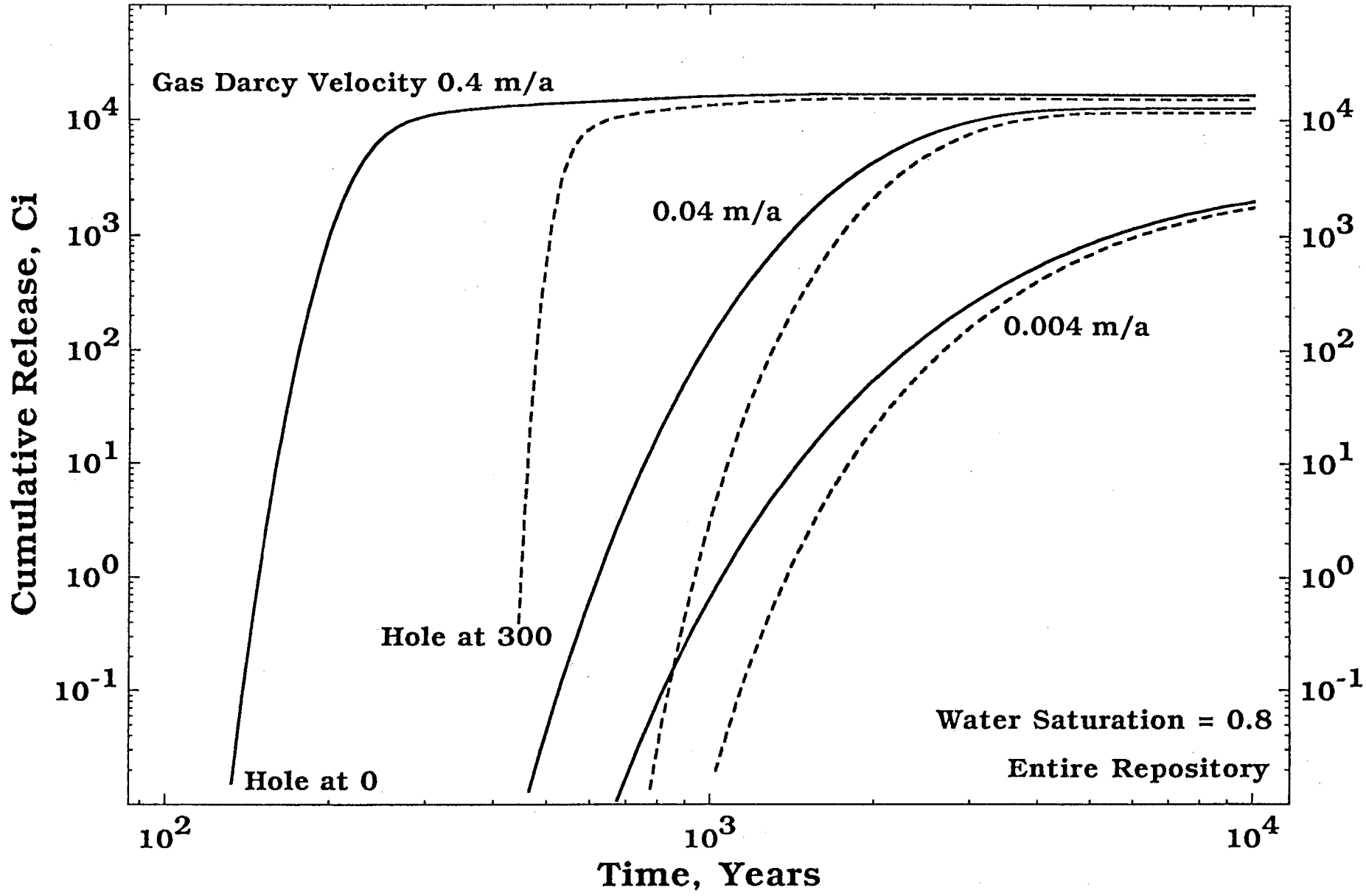

Figure 18. Cumulative Releases of C-14 at Ground Surface, Hole at 0 or 300 Years

LAWRENCE BERKELEY LABORATORY
UNIVERSITY OF CALIFORNIA
INFORMATION RESOURCES DEPARTMENT
BERKELEY, CALIFORNIA 94720